
Electronic Thesis and Dissertation Repository

11-16-2020 2:00 PM

Examining The Structure Of Symbolic Number Representations In The Parietal Cortex: An RSA Study

Aymee Alvarez Rivero, *The University of Western Ontario*

Supervisor: Ansari, Daniel, *The University of Western Ontario*

A thesis submitted in partial fulfillment of the requirements for the Master of Science degree in Psychology

© Aymee Alvarez Rivero 2020

Follow this and additional works at: <https://ir.lib.uwo.ca/etd>



Part of the [Cognitive Neuroscience Commons](#)

Recommended Citation

Alvarez Rivero, Aymee, "Examining The Structure Of Symbolic Number Representations In The Parietal Cortex: An RSA Study" (2020). *Electronic Thesis and Dissertation Repository*. 7438.
<https://ir.lib.uwo.ca/etd/7438>

This Dissertation/Thesis is brought to you for free and open access by Scholarship@Western. It has been accepted for inclusion in Electronic Thesis and Dissertation Repository by an authorized administrator of Scholarship@Western. For more information, please contact wlsadmin@uwo.ca.

Abstract

Previous studies using fMRI adaptation to investigate the neural substrate of symbolic number processing have found ratio-dependent responses in regions of the parietal cortex, suggesting that number symbols are coded by overlapping neuronal populations: the larger the ratio between two numerals, the more their representation overlap. The current study analyzed the distributed patterns of activation associated with numerals presented during this task. I could not find substantial evidence supporting the ratio-dependent structure of the similarity space predicted by the univariate adaptation analyses. I also failed to find evidence in favor of the alternative model that similarities were driven by lexical frequency. These null results were confirmed by Bayesian analysis showing substantial support for the null. These findings do not align with the theory of ratio-dependent overlapping representation of number symbols and challenge previous interpretations of the adaptation literature.

Key Words

Number symbols; fMRI Adaptation; Representational Similarity Analysis

Lay Summary

How are symbolic numerals represented in the brain? Some theories have suggested that numerals are represented in a number line according to their magnitude. Numerals that are closer in this number line are represented in the brain more similarly than numbers that are further away. In other words, the way our brain represents the numeral “3” is more similar to the representation of numeral “4” than numeral “9”. Other authors have suggested that magnitude is not as important in the association between numerals that are established in the brain. These authors have suggested that other factors like frequency are more important. Said differently, this alternative theory poses that numerals that are seen together more frequently in real life are more similar, disregarding their magnitude. In this thesis we tested those competing theories. We could not find evidence for either of them. However, because the first alternative has been highly influential in this research field, our results lead to rethink about these theories. Future studies should develop more advanced models that may determine how numerals are organized in the brain.

Acknowledgements

I would like to extend my gratitude to all the people who contributed to make this thesis possible during such unusual times.

Special thanks to my supervisor, Daniel Ansari, for supporting me and encouraging me all the time. You are a great mentor and an exceptional human being, and I am honored to be part of the NumCogLab family.

I am also deeply grateful to Michael Slipenkyj, for teaching me so much about RSA and for all the effort and the extra hours you put into this project. I couldn't have done it without your support!

I would also like to thank Ian Lyons for collaborating with us and contributing your expertise.

Thanks to all my colleges in the NumCogLab! Lien, Eric, Nathan, Celia, Bea, Mojtaba and Rebekka. I am deeply honoured that I get to work with such an amazing team. Thank you for all the love and support!

Special thanks to Claudia and Liu, my Cuban family in Canada. Clau, you are the best best-friend anyone could ask for. Thank you for having my back since 2008, but specially in the last months. Love you mi ciela!

My deepest appreciation goes to my husband, Carli. Thank you for all your encouragement and love you have given me. The last two years have been an amazing adventure and I'm incredibly happy that I got to spend it with you.

Finalmente, gracias a mi mama y mi papa por el apoyo y el amor incondicional que siempre me dan y por ser "*mi faro y guía*" :D. A mi familia de Cuba, mi tía Tania, mi hermano Dany, mi tío Norvie, mis abuelos y todos los demás, que aunque estén lejos, están conmigo siempre. Esta tesis también es para ustedes.

Table of Contents

Abstract.....	i
Key Words	i
Lay Summary.....	ii
Acknowledgements.....	iii
List of Tables	vi
List of Figures	vii
List of Appendices	viii
1. Introduction	1
1.1. An analog code for the representation of numerical information in the human brain.....	2
1.2. New evidence challenging the tuning curve model	7
1.3. The current study.....	12
2. Methods	15
2.1. Participants.....	15
2.2. fMRI Task and Stimuli.....	16
2.3. fMRI acquisition	17
2.4. fMRI Preprocessing	18
2.5. Predictive models	19
2.5.1. Ratio	19
2.5.2. Frequency	19
2.6. Analysis Plan	20
2.6.1. ROI selection	20
2.6.2. Representational Similarity Analysis	22
2.6.2.1. Deviant to Adaptation Similarity	22
2.6.2.2. Within-Deviant Similarity	26
3. Results.....	31
3.1. Regions of Interest definition	31
3.2. Deviant - Adaptation similarities	34
3.2.1. Effect of Age on the Deviant-Adaptation similarities	38
3.3. Deviant – Deviant Similarities.....	40

3.3.1. Effect of age on the Deviant-Deviant similarities	42
4. Discussion	45
4.1. Predictive value of the Ratio Model	47
4.2. Predictive value of the Frequency Model.....	49
4.3. Age related effects.....	51
4.4. Adaptation vs. Multivariate analysis.....	54
4.5. Implications for future studies.....	56
5. Conclusions	58
6. References	60
7. Appendices	71
8. Curriculum Vitae	80

List of Tables

Table 1. Regions identified with the univariate contrast [Main > Baseline] + [Parametric > Baseline].....	32
Table 2. Regions defined from the probabilistic maps on Juelich Atlas	33
Table 3. Within-Subject polynomial contrasts of repeated measures.	36
Table 4. Within-Subject polynomial contrasts: interaction with Age.....	39
Table 5. Ratio and Frequency model fit.	40
Table 6. Differences between Ratio and Frequency model fit.	42
Table 7. Ratio and Frequency model fit correlation with Age.....	43

List of Figures

Figure 1. Response profiles of numerosity selective neurons in Monkey's prefrontal cortex. Recreated from <i>Nieder & Dehaene (2009)</i>	3
Figure 2. fMRI task and stimuli. Representation of one experimental run.	16
Figure 3. Subdivisions of the IPS according to Juelich Atlas (unthresholded).....	22
Figure 4. Expected pattern similarities between each deviant and the adaptation numeral as predicted by the Ratio (blue) or the Frequency (yellow) model.	24
Figure 5. Deviant – Adaptation similarity analysis	26
Figure 6. (A) Simulated, grayscale representational similarity matrix. (B) Prediction from the Ratio model. (C) Prediction from the Frequency model.	27
Figure 7. Deviant – Deviant similarity analysis plan	30
Figure 8. Significant clusters for the univariate contrast [Main > Baseline] + [Parametric > Baseline]. Coordinates are in MNI space.	31
Figure 9. A. Clusters defined from the IPS subdivisions on Juelich Atlas, including only voxels with $p > .40$; B. Comparison of IPS subdivisions and parietal regions from univariate contrast. Coordinates are in MNI space.	33
Figure 10. Average similarities between each deviant and the adaptation numeral on each ROI included in the analysis	35
Figure 11. Average Similarity Matrices for each region of interest	41
Figure 12. Clusters showing a significant correlation of Ratio Model fit and Age. .	44

List of Appendices

Appendix A. Repeated measured ANOVA (6 Deviants). Within-Subjects Effects.	71
Appendix B. Within-Subjects Polynomial Contrast, after excluding Deviant 12.	72
Appendix C. Within-Subjects Polynomial Contrast using zero-order correlations to estimate similarities.....	73
Appendix D. Within-Subjects Polynomial Contrast interaction with Age, after excluding Deviant 12.....	74
Appendix E. Within-Subjects Polynomial Contrast interaction with Age, using zero-order correlations to estimate similarities.	75
Appendix F. Ratio and Frequency Model fit, after excluding Deviant 12.	76
Appendix G. Ratio and Frequency Model fit, using zero-order correlations to estimate similarity	77
Appendix H. Ratio and Frequency Model fit interaction with Age, after excluding Deviant 12.	78
Appendix I. Ratio and Frequency Model fit interaction with Age, using zero-order correlations to estimate similarity.....	79

1. Introduction

Back in 1967, before the widespread availability of high-resolution neuroimaging, Moyer and Landauer (Moyer & Landauer, 1967) used a simple number comparison task to investigate the cognitive underpinnings of symbolic number processing. They found that participants are faster and more accurate comparing two numerals that are relatively far apart (e.g., 1 and 9) compared to numerals that are closer together (e.g., 7 and 8). Moreover, for a fixed distance, comparison of relatively smaller numbers (e.g., 1 and 2) was also found to be faster and less error-prone, relative to larger ones (e.g. 8 and 9). Such behavioral signatures of symbolic number comparison, known in the literature as the distance and size effect, have been replicated numerous times since then (e.g. Ansari et al., 2005; Dehaene et al., 1990; Duncan & McFarland, 1980; Holloway & Ansari, 2009; Van Opstal et al., 2008). These results suggest that mental representations of numerical magnitude do not follow the formal rules of the symbolic system, in which the difference between 3 and 4 is exactly the same as the difference between 8 and 9. Instead, it appears as though such numerical computations are supported by an analog code in which the accuracy of the representation decreases as magnitude increases. In this compressed representation, the difference between any two numerals is determined by their ratio, as described by Weber's Law.

A large volume of research has studied this analog system directly (Cantlon & Brannon, 2006; Dehaene, 1992; Feigenson et al., 2004; Gallistel & Gelman, 1992; Halberda & Feigenson, 2008), using non-symbolic discrimination tasks (i.e., comparing or ordering sets of dots). These studies found that, when counting is not possible, humans' ability to discriminate between two patterns of dots also depends on their ratio.

These experiments typically control the physical properties of the stimuli used. Hence, most researchers agree that such comparisons are supported by neural networks specialized for the perception of magnitude information from the environment (but see Leibovich et al., 2017).

This module seems to exist from infancy onwards. Specifically, the same type of non-symbolic discrimination abilities has also been demonstrated in pre-verbal infants (Xu & Spelke, 2000) and non-human primates (Cantlon, 2012; Cantlon & Brannon, 2006). These studies have revealed very similar behavioral signatures across phylogeny and ontogeny: human adults, children and animals alike, are slower and more error prone as the ratio between the two magnitudes (calculated as smaller/larger) gets closer to 1. This consistency of the ratio effect has further supported the idea of an evolved capacity for magnitude discrimination in the human brain, grounded on neural circuits that represent magnitude in a logarithmic, compressed scale.

1.1. An analog code for the representation of numerical information in the human brain

Studies trying to uncover the neural basis of this analog, magnitude code have identified a system of numerosity selective neurons on the monkey brain, along regions equivalent to the human prefrontal cortex (PFC) and parietal cortex (PC) (Nieder et al., 2002; Nieder & Miller, 2003). The response pattern of these neurons is characterized by a gaussian tuning curve. The center of the curve represents the numerosity to which the neuron responds preferentially. The width represents the noise in the response; namely, the degree in which other magnitudes, different from the preferred one, also activates

the neuron. Together, these neurons form a system of overlapping representations that code numerosity in an imprecise way (Figure 1). As the magnitude increases, so does the noise in the representation and thus, the overlapping between the neurons.

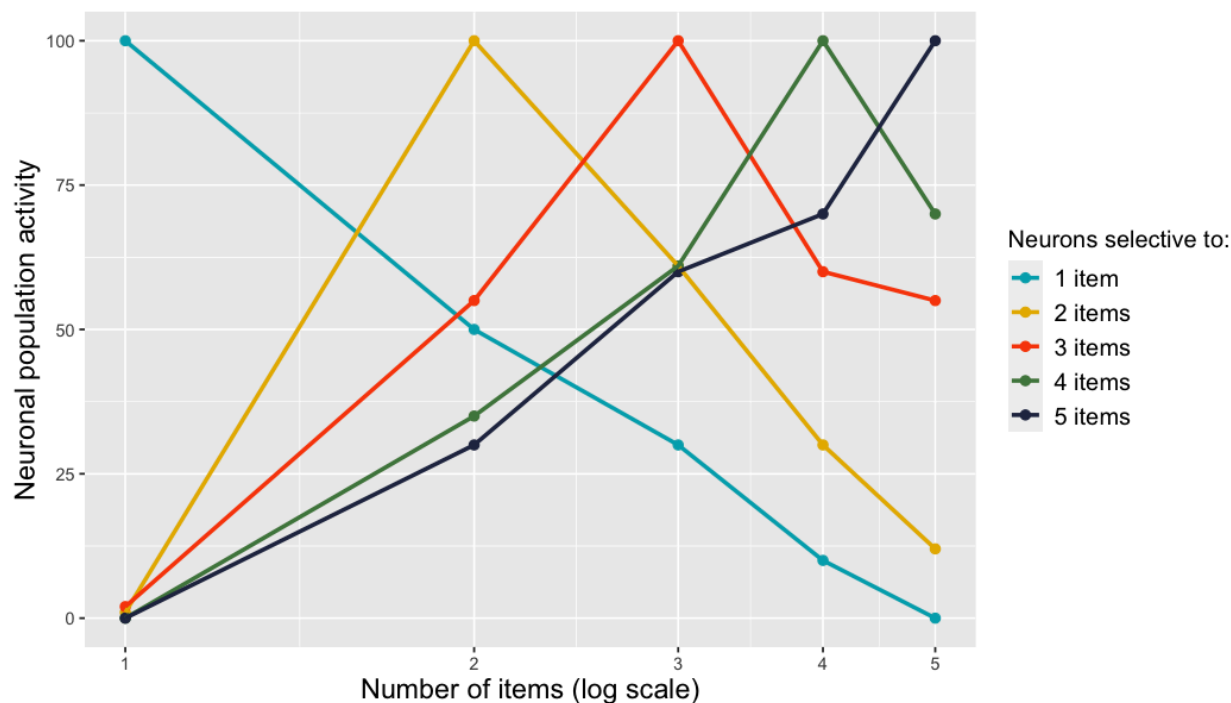


Figure 1. Response profiles of numerosity selective neurons in Monkey’s prefrontal cortex. Recreated from Nieder & Dehaene (2009).

To test whether such system may be the base for later symbolic knowledge, researchers trained monkeys to associate dot patterns with corresponding number symbols (Diester & Nieder, 2007). Once the association was established, the authors measured the responses of single neurons across PFC and PC to the presentation of either the dot arrays or the symbols. They were able to identify “association” neurons that responded to the abstract magnitude information, disregarding the presentation

format. These results provide indirect evidence that such distributed population code of magnitude identified in the monkey is a plausible evolutionary precursor of humans' advanced, symbolic numerical abilities.

By using functional Magnetic Resonance Imaging (fMRI) techniques, researchers have tried to test more directly whether a similar system for magnitude discrimination can be identified in the human brain. In particular, neuroimaging studies have identified regions across the parietal cortex that are consistently active during both symbolic and non-symbolic tasks (Holloway et al., 2010; Holloway & Ansari, 2010).

In order to reveal the underlying representation that may be hosted in these regions, researchers have used paradigms such as fMRI adaptation. During a typical fMRI habituation paradigm, a monotonic decrease in the blood-oxygen-level dependent (BOLD) signal is observed as a result of the repeated presentation of a particular stimulus (Grill-Spector & Malach, 2001). After this habituation phase, a variation of one of the properties of the stimuli is introduced. Functional properties of different neuronal populations can be inferred by measuring their response -or lack of- to this change. Namely, a rebound in the BOLD signal should be observed across those regions containing populations of neurons that are sensitive to the feature that was varied. Hence, the less overlap between the deviant stimuli and the adapted one, the larger the rebound that is obtained (Grill-Spector, 2006).

Using this paradigm, Piazza et al. (2004) found repetition suppression effects across the parietal cortex while participants looked at different dot patterns with the same numerosity (e.g., 16 dots). Critically, when this habituation phase was interrupted by an array of dots with different numerosity (e.g., 32), a distance-dependent recovery

of the activation was observed across bilateral intraparietal sulci. In other words, the rebound in the BOLD signal was larger as the deviant was numerically further away from the habituation stimuli (e.g. larger for 32 than 18). These effects are consistent with a system for approximate magnitude processing in humans, similar to the one identified in monkeys, in which numerosities that are closer have more overlapping representation and thus, are harder to discriminate.

Moreover, based on the behavioral data showing that performance on both symbolic and non-symbolic comparison is modulated by the ratio of the magnitudes, researchers have argued that symbolic numerals inherit the same representational code of their non-symbolic counterparts (Piazza, 2010; Piazza et al., 2007). Recent studies using a similar fMRI adaptation paradigm suggest that this may be the case (Goffin et al., 2019; Holloway & Ansari, 2010; Notebaert et al., 2010; Vogel et al., 2015, 2017). Specifically, in these studies, researchers used a symbolic version of Piazza's adaptation design. Instead of dot arrays, habituation effects were triggered by the repeated presentation of a symbolic numeral (e.g., number "6"). The habituation phase was then interrupted by a numerical deviant (e.g., number "9"). Similar to the Piazza study, by varying the numerical magnitude of the deviants in a parametric fashion, these studies have successfully identified a subregion of the parietal cortex (the intraparietal sulcus; IPS) where activation decreases during the adaptation phase and rebounds after the presentation of deviants. Critically, the recovery of the activation is a function of the numerical ratio between the adaptation and the deviant number: the larger the ratio between two numerals, the smaller the signal recovery in the IPS. These results are consistent with the tuning curve model. Under this model, neurons responding to

numeral 6 also respond, in less degree, to numeral 5 and vice versa. Because of that, a portion of the neurons coding for numeral 5 also get adapted during the habituation phase and only the remaining, non-shared portion detects a change when deviant 5 is presented. As the ratio between deviant and adaptation stimuli decreases, so does the proportion of shared neuronal populations and thus, a larger response to the deviant is observed. These results represent strong evidence in favor of an analog code underlying the processing of symbolic numerals.

Contrary to non-symbolic stimuli, in which the physical properties of the dot patterns cannot be fully controlled and may represent a confound, there is nothing in the visual shape of the numerals that may fully explain such ratio-dependent recovery (but see Cohen, 2009). In fact, the semantic nature of this effect has been confirmed by further replications of this paradigm in a cross-linguistic sample -using Arabic numerals and Chinese Ideographs- showing that this effect only occurs when participants know the meaning of the symbols (Holloway et al., 2013).

In summary, the parallel between behavioral and neuroimaging ratio signatures during both symbolic and non-symbolic processing has been taken as evidence of a unique abstract representation of numerical information. This has been one of the most influential theories in the field of numerical cognition, with significant implications for our understanding of how symbolic numerals are represented in the brain.

1.2. New evidence challenging the tuning curve model

Despite the popularity of the tuning curve model as a plausible code to represent number symbols, the key ideas at the core of this theory are currently been subject of debate (see Leibovich & Ansari, 2016; Reynvoet & Sasanguie, 2016; Wilkey & Ansari, 2020 for detailed reviews) as some researchers have failed to find support for some of the predictions that can be derived from this theory. For example, if there is indeed a unique abstract code to represent both symbolic and non-symbolic magnitudes, conversion between both formats should be a relatively easy, if not automatic, process. To put this idea to the test, Lyons et al. (2012) presented participants with a comparison task that included three different conditions: a non-symbolic comparison, a symbolic comparison, and a mixed-format comparison. The authors hypothesized that a strong link between numerals and their corresponding analog magnitudes would result in a very low cognitive cost of the mixed comparison. However, their results point in another direction. Numerical comparisons across different formats were always less accurate and slower than comparisons within the same format, an effect that could not be explained by the differences of visual properties. These results do not support the existence of a strong mapping between both systems, at least during adulthood, although the authors do not rule out the possibility of such link during the first stages of learning.

In addition to the behavioral evidence, the availability of new multivariate analysis methods, have provided new information about the distributed patterns of activation across specific brain regions when participants are presented with numerical information. While traditional univariate analyses have provided insights into which brain

regions may play an essential role in the representation of numerals, the fine-grained information about the distributed activation of individual voxels is usually lost as activation is averaged across whole regions. In contrast, multivariate methods allow researchers to test whether activation of similar regions across non-symbolic and symbolic processing results from similar representations or the coexistence of different neuronal populations with different properties across the same regions.

Studies using machine learning methods to analyze brain activity during number processing tasks have confirmed that magnitude information can be decoded from the activation of parietal regions, for both symbolic and non-symbolic stimuli (Bulthé et al., 2014, 2015, 2018; Damarla & Just, 2013; Eger et al., 2009; Wilkey et al., 2020). Consistent with the tuning curve model, some studies also found that decoding accuracy between non-symbolic arrays increased with numerical distance (Bulthé et al., 2014; Eger et al., 2009). However, surprisingly, the same effect was not observed for symbolic numerals.

Another critical question that these studies have addressed is whether algorithms trained to identify numerosity from one format can accurately classify stimuli on the other format. If there is a unique, analog representation of numerals underlying both symbolic and non-symbolic stimuli, then we should expect considerable overlap between the patterns across both formats, resulting in a high level of cross-format classification. Results from studies testing this prediction have not been consistent, with some authors reporting some degree of cross-format classification (Damarla & Just, 2013; Eger et al., 2009), while other not (Bulthé et al., 2014, 2015). For example, Eger et al. (2009) found that classifiers trained on non-symbolic stimuli did not generalize to

symbolic stimuli. However, when classification was attempted in the other direction, from symbolic to non-symbolic, they did observe some degree of generalization, however the accuracy was lower than 60% (chance = 50%). In a more recent study, with a larger sample size, Wilkey et al. (2020) found cross-format generalization in both directions, from symbolic to non-symbolic stimuli and vice versa. However, as the authors point out, this data suggest the existence of shared neural resources across both formats at a certain spatial scale; however, it cannot establish whether both representations completely overlap.

On the other hand, studies using Representational Similarity Analysis (RSA, Kriegeskorte, Mur, & Bandettini, 2008) have found very low correlations between the neural patterns of activation associated with numerals and dot arrays (Lyons et al., 2015a). This method also allows researchers to compare how the observed pattern of similarities between individual stimulus fits different theoretical predictions. For example, these studies have confirmed that similarities in the distributed patterns of neural activity along parietal regions when participants are presented with non-symbolic stimuli can be predicted by ratio (Lyons et al., 2015a; Lyons & Beilock, 2018). This is in line with the tuning curve model for the representation of analog magnitudes. The larger the ratio between two numbers, the larger the similarity in the distributed patterns as a result of a larger overlap between the populations of neurons tuned to each numerosity. In contrast to the non-symbolic number processing data, Lyons et al reported that the ratio model does not fit the geometry of similarities when processing symbolic numbers. Moreover, when comparing the neural patterns of the symbolic numerals, researchers found near

zero correlation between them, suggesting that symbols are represented independently from one another (Lyons et al., 2015).

In summary, while there seems to be evidence favoring the tuning curve model to represent non-symbolic magnitudes in the human brain, direct proof of this being the system that supports the representation of number symbols has not been reported. Critically, some studies have demonstrated that distance and ratio effect during number comparison can also appear due to other factors, such as differences in stimulus frequency. It is known that the probability of encountering an Hindu-Arabic digit does not follow a uniform distribution (Benford, 1938; Dehaene & Mehler, 1992). In a study measuring the regularities in the frequency of numerals across different languages, Dehaene and Mehler quantified those probabilities and found a consistent decrease in the frequency of numerals with increasing magnitudes. Some authors have hypothesized that because small numerals are considerably more frequent in our daily interactions with the environment, their representation may be more accurate. To test this hypothesis, Krajsci et al. (2016) used a paradigm in which participants had to learn new numerical symbols and manipulated the frequency distributions. They found that size effects during numerical comparison tasks using the newly learned symbols only appeared when the frequency of presentation of the symbols was uneven. Consistent with these results, one recent study using RSA found that similarities in the patterns of activation associated with individual numerals along the parietal cortex are better predicted by frequency of co-occurrence, rather than ratio (Lyons & Beilock, 2018). These results raise the need to revisit previous neuroimaging evidence about the neural representation of numerals. Critically, if other factors such as frequency may explain the

behavioral signatures observed in symbolic comparison, it is possible that it also explains effects on brain activation, such as the ratio-dependent recovery observed in the IPS during adaptation paradigms.

While the existence of some degree of overlap between symbolic numerals and analog magnitudes in parietal regions cannot be completely ruled out, the link between these two representations may be more dynamic than previously hypothesized. As has been proposed by some authors, it is possible that associations between both systems only occur during initial stages of learning (Lyons et al., 2012), or are limited to really small numerosities (Reynvoet & Sasanguie, 2016). During development, as the more abstract properties of numerals become more relevant for more complex math abilities, initial links between symbols and magnitudes may be gradually replaced by other, more relevant symbol-symbol associations. Alternatively, features of the symbolic system such as order and differences in frequency distributions may bias the learning process from the very beginning.

The combination of experimental paradigms that can accurately capture developmental changes in the brain, combined with the new methods for fMRI multivariate data analysis may help to answer these questions. However, our ability to study how representations of numerals change across development and learning is constrained by the limitations of current neuroimaging techniques. When participants of different ages are asked to complete a task within the scanner, it is hard to discriminate whether observed changes are due to a refinement of the representation of numerical information or other general domain processes such as age-related differences in reaction times or task comprehension (Poldrack, 2000). Passive paradigms, such as the

ones described above, are a suitable alternative to this limitation, since they disconfound developmental changes in behavior from age-related changes in the underlying neural representation (Nordt et al., 2016).

One important argument in favour of this fMRI adaptation paradigm with symbolic numerals relies on the consistency of the results across multiple, independent replications. The ratio-dependent recovery of the signal appears with either small or large numbers (Notebaert et al., 2010), visual or auditory presentation modalities (Vogel et al., 2017), children or adults (Goffin, 2019; Vogel et al., 2015). This body of research provides a strong foundation for the use of this design to study automatic responses to numerals in the absence of explicit task demands and raises the need to understand better the neural mechanisms that cause this effect.

1.3. The current study

With the current study, I aimed to understand better the neural basis of symbolic numbers representation and associated developmental changes. Specifically, I carried out a secondary analysis of an open fMRI data set including 45 children from ages 6 to 14 (Goffin, 2019). In particular, this study used a method known as fMRI adaptation to glean insights into the neural correlates of symbolic number processing and age-related differences therein. In the original study, the authors found neural habituation effects across parietal regions during the repeated presentation of a symbolic numeral; followed by a ratio-dependent rebound of the signal after the presentation of a deviant. In order to better understand the neural mechanism at the base of this effect, the current study will use a Representational Similarity Analysis (Kriegeskorte, Mur, &

Bandettini, 2008) to assess the distributed patterns of activation generated by the numerical deviants across specific regions of the brain and the changes that occur in this representation across development.

Specifically, I tested whether the ratio-dependent rebound of the BOLD signal observed at the univariate level translated into ratio-dependent similarities at the multivariate level. If the overlap between the populations of neurons coding for specific numerals is consistent with the tuning curve model - as has been hypothesized in the past - we should expect this to be true. In other words, deviants that are closer to the adaptation stimuli (larger ratio) should have more overlapping representations and, therefore, elicit a more similar pattern of activation than those that are further away.

Additionally, I examined whether the pattern of similarities between the numerals is driven by their lexical frequency. Since we know that smaller numerals are more frequently encountered in real life, the probability of any two small being together is higher than that of two larger numerals. As a result, smaller numerals may have more similar representations than larger numerals. Recent studies suggest this is a better model to predict similarities between the neural representation of numerals along the IPS (Lyons & Beilock, 2018). However, those results come from the analysis of neural responses in the adult brain and thus, may reflect only the end state of a representation which is gradually constructed and refined over the course of learning and experience. The present study extended those findings by testing whether this model is also a good predictor of the similarity space during the initial years of learning, or whether this frequency-based structure is only gradually established as a result of the interactions with numerals across development. In addition, in contrast to Lyons et al. (2018) who

used a number matching task, the present study analyzed patterns of activation in response to numerals during a passive paradigm. Previous studies have shown that activation of parietal regions during this paradigm is sensitive to the magnitude information being presented, even though participants are not required to perform any numerical judgment.

2. Methods

2.1. Participants

The data used for the current analysis was originally collected by Goffin (2019). They recruited children across 9 different age points, ranging from 6 to 14 years old. The final sample included 45 participants (18 females, $M_{Age} = 125.44$ months, $SD_{Age} = 31.46$ months), 5 per age group. In order to reach this number of valid datasets, researchers had to recruit a total of 65 children. Twenty participants had to be excluded from the analysis according to pre-registered criteria (available at: <https://osf.io/amuc5/>). For the current analysis, I used the same inclusion parameters as the original study.

Participants had to be healthy, right-handed, fluent-English speakers. On each functional run participants had to meet the minimum accuracy (at least 75%) and head motion criteria ($< 3\text{mm}$ across run and $< 1.5\text{mm}$ volume-to-volume displacement). Runs that did not meet these parameters were left out of the analysis. Because of that, some participants only contributed 2 or 3 functional runs to the final dataset. Participants with less than 2 valid runs were excluded completely. In addition, two participants were able to complete 5 runs of the task. In those cases, accuracy and head motion was assessed for each run and only the four best were included in the analysis. As a result, a total of 161 valid data sets were included in our analysis.

2.2. fMRI Task and Stimuli

Functional data was collected while participants completed 4 runs of a symbolic-number adaptation task. The task consisted of several repetitions of the numeral 6, consistently interrupted by a deviant (Figure 2). The length of the repetition phase was varied across the run, ranging from 5 to 9 repetitions (overall mean of 7), to create a jitter in the interval between deviants and oversample the hemodynamic response. Deviants were selected according to their ratios relative to number 6, calculated as smaller / larger numeral. Deviants 3 and 12 represented the Small Ratio condition (ratio = .5). Deviants 4 and 9 represented the Medium Ratio condition (ratio = .67). Finally, deviants 5 and 8 represented the Large Ratio condition (ratio = .75 and .83, respectively). During a single run, there were three repetitions of each deviant (for a total of 18 numerical deviant trials).

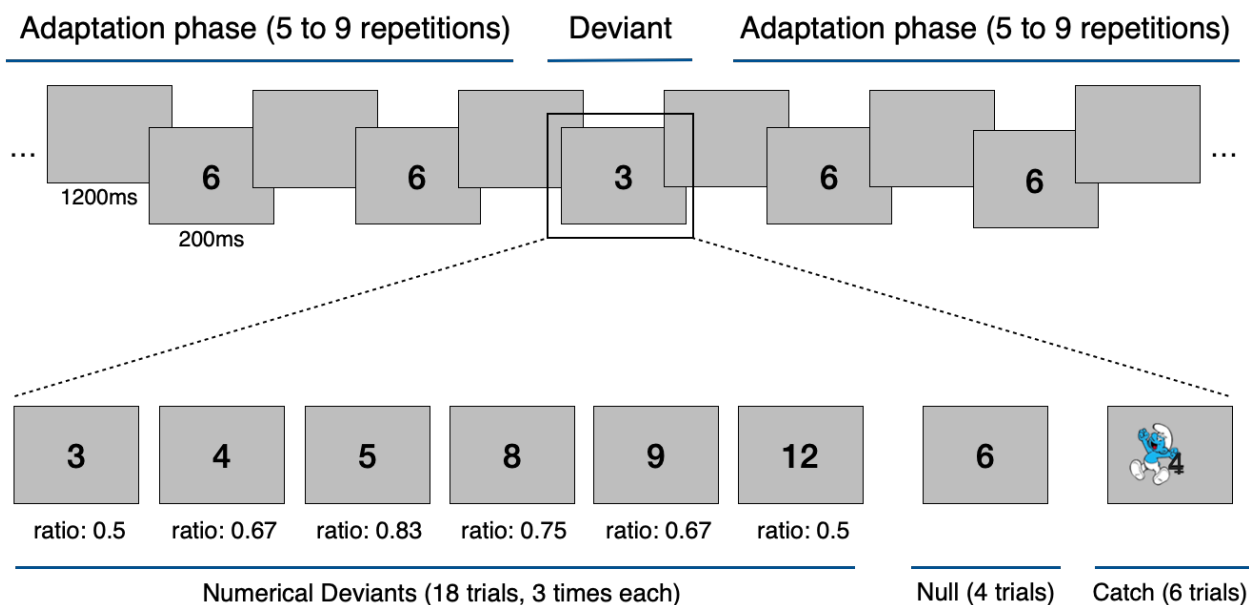


Figure 2. fMRI task and stimuli. Representation of one experimental run.

In addition to these deviants, the adaptation phase could also be interrupted by either a catch trial (8 per run) or a null trial (4 per run). Catch trials consisted of any of the deviant numerals but accompanied by a Smurf. Participants were instructed to respond to these trials with a button press, using their right hand. Null trials consisted of yet another presentation of the adaptation numeral and thus, they look identical to the adaptation phase. During the analysis, these trials will be used to estimate the neural activation corresponding to the numeral 6. The order of presentation of different trials types was randomized across the run. Catch trials in particular were pseudo-randomized so participants could not predict their presentation, but they were never next to each other.

Across the whole experiment, the stimuli were presented during 200ms, interspersed with a blank screen with a duration of 1200ms. To avoid adaptation effects related to low-level properties of the stimuli both font and screen location were varied consistently during the experiment. Additional details about the procedure could be found on Goffin (2019).

2.3. fMRI acquisition

Anatomical and functional MRI data was collected with a 3T Siemens Magnetom Prisma scanner using a Siemens 32-channel head coil. To collect fMRI data, a BOLD-sensitive T2* weighted echo-planar sequence was used. Each volume included 48 slices that covered the entire brain (voxel size = 2.5mm x 2.5mm x 2.5mm, 2.5mm thickness, TR = 1000ms, TE = 30ms, multi-band factor = 4, FOV = 208x208mm, matrix size = 84 x 84, flip angle = 40°. The slices were collected in an ascending-interleaved

method. A total of 386 volumes were collected for each run of the adaptation task. The anatomical data was collected using high-resolution T1-weighted images in the sagittal plane (voxel size = 1mm x 1mm x 1mm, TR = 2300ms, TE = 2.98ms, TI = 900ms, flip angle = 9°, in-plane resolution = 256mm x 256mm). A total of 192 slices covering the whole brain were collected.

2.4. fMRI Preprocessing

Imaging data was pre-processed using BrainVoyager, version 20.6 (Brain innovation, Maastricht, the Netherlands; Goebel et al., 2006). Anatomical images were skull separated, corrected for intensity inhomogeneities and transformed to MNI space. Functional data was processed using slice scan-time correction using cubic spline interpolation, low frequency drift removal using a high-pass filter with a 2 cycles cut-off (GLM with Fourier basis set), 3D head motion correction using trilinear/sinc interpolation. Spatial smoothing was applied only for the univariate contrasts (6mm FWHM Gaussian kernel); the multivariate analyses were performed on unsmoothed data. Finally, functional and anatomical data were co-registered to the same space (gradient-based registration) and functional images were resampled to 3mm isotropic voxel.

The stimuli presented during the experimental task were modeled into a GLM and convolved with a two-gamma hemodynamic response function. Different GLM's were used for the ROI selection procedure and the RSA analysis, as specified down below.

2.5. Predictive models

2.5.1. Ratio

The numerical ratio between numerals was calculated as $[\text{ratio} = \min(n_1, n_2) / \max(n_1, n_2)]$. This model assumes equivalent activation patterns for deviants below or above the adaptation numeral, provided that the ratio is the same.

2.5.2. Frequency

The frequency with which each number appears in everyday life was calculated according to Benford's Law (Benford, 1938). This law describes accurately the probability of encountering a numeral n in the first (leftmost) position of a number as: $p = \log_{10}(n+1) - \log_{10}(n)$. In a subsequent study, Dehaene and Mehler (1992) tested is whether the law can in fact be used to predict the frequencies of numbers as a whole, rather than digit positions. They found that the law does provide a very accurate estimate of the frequency of single-digit numerals. This estimation of frequency is highly correlated with number size: smaller numerals are more frequent than larger ones.

However, it should be noted that Benford's Law does not accurately predict certain peaks in the frequency distribution of numerals that are frequently used in approximation contexts, such as 10, 12, 20 or 100. As a result, it is unclear what would be the exact estimation of frequency value for the numeral 12 included in our task. Given the lack of either raw data or a specific algorithm to estimate this probability, and for the sake of simplicity, I used Benford's Law as an approximation for the frequency of numeral 12. Throughout all the analyses, I tested whether excluding this numeral from the analyses had an impact on the results.

Finally, in order to predict pattern similarity on any two numerals based on this model, I calculated a joint frequency measure. This is, the product of the numeral's individual probabilities. This procedure is similar to the one used by Lyons & Beilock (2018).

2.6. Analysis Plan

A complete analysis plan was elaborated and preregistered before having access to the neuroimaging data (pre-registration can be found at <https://osf.io/t4jb3/>). The following sections contain the description of all the pre-registered procedures.

2.6.1. ROI selection

Two different criteria will be used for ROI selection. First, a univariate contrast will be run on the smoothed data (6mm kernel) in order to identify regions that respond to the presentation of the deviant events (See Figure 2 above). The GLM used for this analysis will include two main regressors: one for the main effect of change, in which all deviants are assigned the same weight; and one parametric regressor, in which deviants are weighted differently according to their ratio to the adaptation stimuli (the repeated 6's). In addition, catch and null trials will be included in the GLM as predictors of no interest. The adaptation phase will be modeled as baseline.

Regions of interest will be selected using the conjunction [Main effect > Baseline] + [Parametric effect > Baseline]. With this conjunction I am aiming to identify regions that respond to the change introduced by deviants in a meaningful way, avoiding areas that respond to low level changes or possible spurious parametric effects. In other words,

this conjunction identifies regions that are both modulated by the presentation of the deviants and that are correlated with the ratio between the deviant and the habituation stimuli. Initially, significant clusters will be identified using an uncorrected threshold of $p < .001$ and then corrected for multiple comparisons at the cluster level using Monte Carlo simulations (1000 iterations) at $p < .05$ (Forman et al., 1995). In order to make results more interpretable, large clusters will be split into smaller regions using a k-means clustering algorithm (Lloyd, 1982) implemented in Matlab (version 9.5.0.1298439, R2018b). This conjunction analysis is similar to previous studies describing the parametric recovery of the BOLD signal in response to deviants across the parietal cortex (Goffin, 2019; Vogel et al., 2015). With this part of the analysis, I aim to characterize the multivariate properties of the regions showing this particular effect.

In a second set of analyses, I will use an independent ROI selection method. Specifically, I will include the subregions of the IPS defined by the Juelich Atlas probability maps (Figure 3). This atlas defines three different subdivisions of IPS: IP1, IP2 (Choi et al., 2006) and IP3 (Scheperjans, Eickhoff, et al., 2008; Scheperjans, Hermann, et al., 2008). These subdivisions were defined taking into account the cytoarchitectonic properties of the tissue, which makes them well suited to test hypotheses about brain function. To avoid overlapping between the probability maps, only those voxels with at least a 40% probability of being part of a subdivision will be included in the ROIs. Excluding the voxels with lower probabilities should result in an increased anatomical precision, while providing an accurate estimate of the real size of the subdivision (Eickhoff et al., 2006).

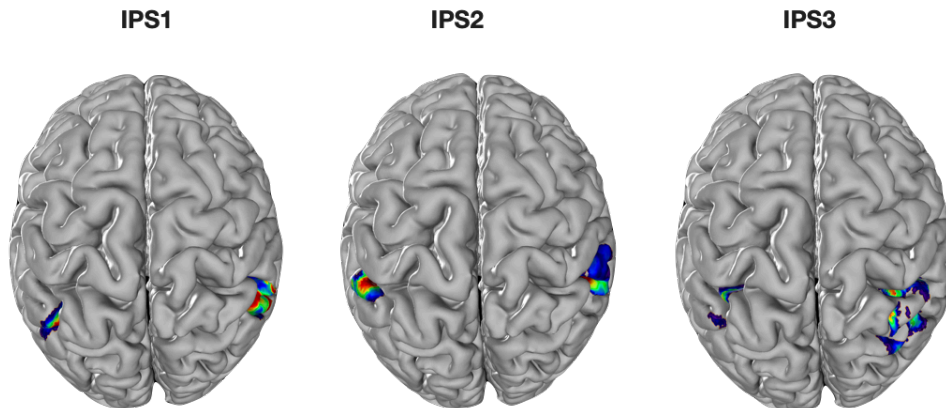


Figure 3. Subdivisions of the IPS according to Juelich Atlas (unthresholded)

2.6.2. Representational Similarity Analysis

In order to obtain the activity estimates that will be used for the Representational Similarity Analysis, I will run an RFX GLM on the unsmoothed functional data including separate regressor for each of the six deviants, one regressor for null trials and one regressor for catch trials. The pattern of neural activation will be assessed by extracting beta values for each condition in the functional voxels (3x3x3mm) in each ROI.

In each individual ROI, the similarities between the patterns will be tested during two separate analyses. In the first part the similarities between each deviant and the adaptation numeral will be assessed. This analysis is the multivariate equivalent of the traditional Deviant VS Adaptation contrast that has been done by previous studies. In the second part, the similarities between deviant numerals only will be tested against our conceptual models.

2.6.2.1. Deviant to Adaptation Similarity

For the first part of our analysis (full analysis plan depicted in Figure 5), the activity patterns corresponding to each of the six deviants and the adaptation numeral will be

compared in each individual ROI. The pattern associated with the adaptation numeral will be estimated using the data from null trials, not the baseline adaptation phase. As a result, comparisons between this pattern and that of numerical deviants should not be biased by the [Deviants > Baseline] contrast used during the ROI selection procedures (see Kriegeskorte et al., 2009). In addition, keeping the adaptation phase as baseline would be consistent with previous univariate contrasts performed on this data, which will make results more comparable.

Representational similarities within a particular ROI will be estimated using Pearson's r . The beta maps corresponding to each number will be vectorized and then, the correlation between the vectorized maps of each deviant and numeral 6 will be computed. These will be partial correlations, as catch trials will be included as covariates. While catch trials also include a motor component (participants are supposed to press a button in response to this trials), they share with the rest of the stimuli other task related components. Controlling for these trials would give us the opportunity to isolate the activity uniquely related to the representation of numerals. However, zero-order correlations will be computed as well and relevant changes in the results will be reported. Since Pearson's r values are not normally distributed (values range from -1 to 1), the obtained correlations will be normalized using a z transformation ($z = \text{arctanh}(r)$) in order to use them as input for further statistical analysis.

For a given ROI, the similarities values (normalized correlations) obtained on each participant will be analyzed at the group level using a repeated-measures ANOVA with polynomial contrast. Figure 4 represents the two main predictions for this analysis. If a larger ratio between the deviants and the adaptation numeral is associated with

higher similarities in the underlying patterns of activation (Hypothesis 1), we should expect a significant quadratic trend (blue line). Under this model, the mean similarities between deviants in the same ratio bin should be equal.

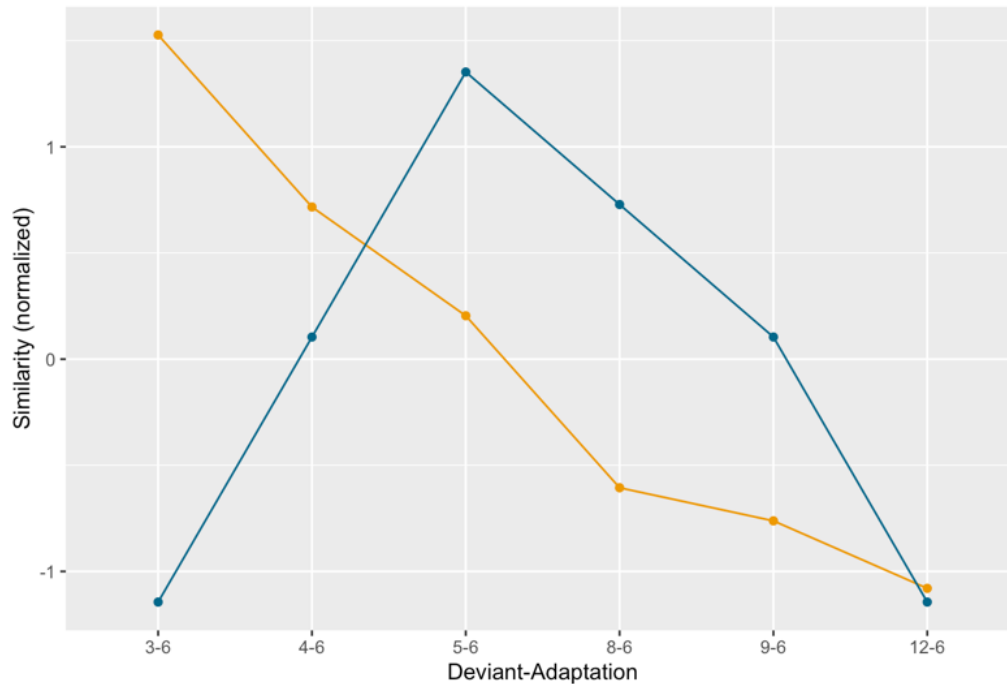


Figure 4. Expected pattern similarities between each deviant and the adaptation numeral as predicted by the Ratio (blue) or the Frequency (yellow) model.

On the other hand, if the similarities are predicted by the joint frequency of numerals (Hypothesis 2), then we should expect a significant linear trend (yellow line), indicating a decrease of the similarities as the magnitude of the deviant increases. To confirm that pattern, I will test whether, for a given ratio, similarities of the deviants

below the adaptation numeral are significantly larger than the ones above (Hypothesis 2.1) using a t-test with significance level of $p < .05$.

Finally, follow-up analysis will be done to test the effect of the participants' chronological age (Hypothesis 1.1 for the ratio model; Hypothesis 2.2 for the frequency model). To do that, I will repeat the ANOVA analysis but adding age as a between-subjects factor. For all of our analysis, I will report our results at the uncorrected threshold of $p = 0.05$, but also using a Dunn-Sidak correction for multiple comparisons (Šidák, 1967), in which the alpha level is adjusted according to the number of independent ROIs.

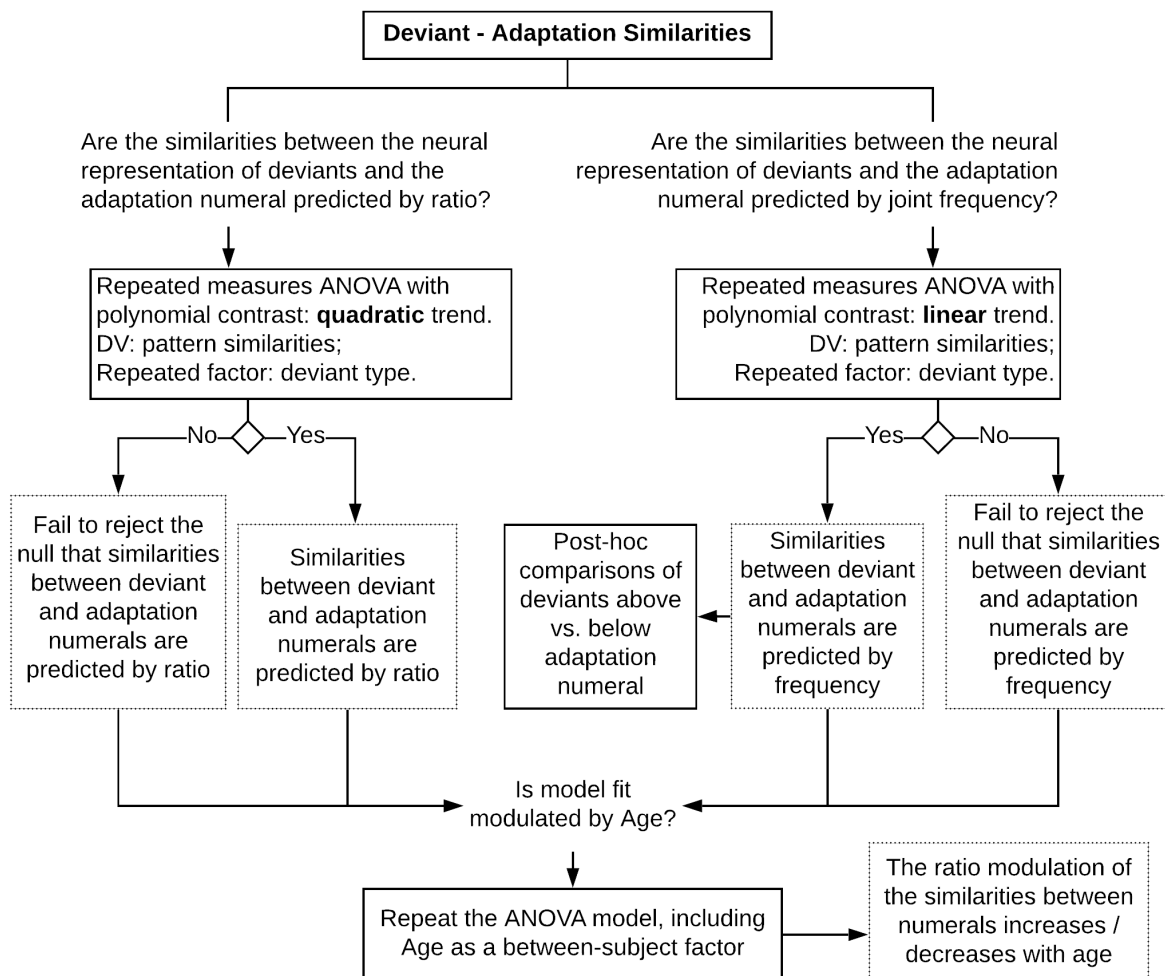


Figure 5. Deviant – Adaptation similarity analysis

2.6.2.2. Within-Deviant Similarity

Next, the activity patterns corresponding to deviant numerals only will be compared on each individual ROI (full analysis plan depicted in Figure 7). The similarity between patterns will be calculated using Pearson's r correlations. This is, all possible pairwise correlations between the vectorized beta maps corresponding to each deviant will be computed. Since all the deviants are presented after a repeated stream of

numeral 6, null trials will be included as a covariate. This would allow us to remove influence of previous presentations of the adaptation numeral from the pattern and isolate the effects specific to each individual deviant. However, zero-order correlations will be reported as well. The obtained correlations will be also normalized here, using a z transformation, where $z = \text{arctanh}(r)$.

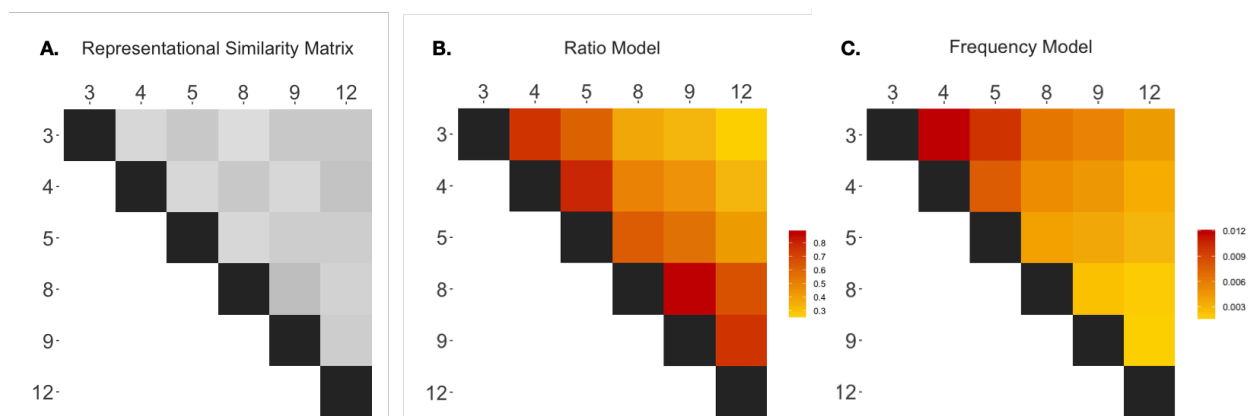


Figure 6. (A) Simulated, grayscale representational similarity matrix. (B) Prediction from the Ratio model. (C) Prediction from the Frequency model.

For each individual participant, a Representational Similarity Matrix (RSM, Figure 6A) will be built, containing all pairwise normalized correlations. This matrix is then tested against predictions built from a Ratio (Hypothesis 3; Figure 6B) and a Frequency model (Hypothesis 4, Figure 6C), using Pearson's r . The obtained correlations between participants' RSM and each of the two models are then z-transformed and analyzed at the group level using a one-sample t-test to determine whether they are significantly different from zero. If neural activity fits the predictions from the model, then we would expect that the correlation between the individual RSM's and the model should be

significantly larger than 0. On the other hand, a significant negative correlation would indicate neural encoding in the opposite direction as the model prediction.

This procedure is repeated across each ROI. Model fit significance will be reported using both an uncorrected alpha of $p < .05$, and after correcting for multiple comparisons also using a Dunn-Sidak method (Šidák, 1967) in which the alpha level is adjusted according to the number of ROIs.

Next, I will compare model fit of the Ratio and the Frequency model by running a two-sample t-test on the model fit values, using a significance level of $p < .05$. This would allow me to test whether one model described the neural encoding of numerals significantly better than the other (Hypothesis 5).

For any region in which model fit is non-significant, I will run Bayesian one sample t-test using JASP software, Version 0.12.2 (JASP Team, 2019), in order to calculate the amount of evidence in favour of the null hypothesis (the mean correlation between the neural representation is and the model is zero). Support for the null model (that the mean similarities between all deviants and the adaptation stimuli are equal) will be estimated using Bayes Factor (BF). Results will be interpreted using the guidelines from Jarosz & Wiley (2014): BF between 1 and 3 = weak/anecdotal support (not enough evidence to make any substantial claims either for or against the predicted relationship); BF between 3 and 10 = substantial support (enough evidence to make moderate claims about effect); BF between 10-100 = strong evidence (enough evidence to be make moderate/strong claims about effect); BF greater than 100 = very strong/decisive evidence (enough evidence to make strong claims about effect).

Regardless of significance, I will test whether model fit can be predicted from participants' chronological age (Hypothesis 3.1 for the Ratio model; Hypothesis 4.1 for the Frequency model). In other words, I will try to answer the question of whether the predictive value of each of our conceptual models changes across age. To do that, I will use the model fit measures obtained before for each participant (normalized correlations between the RSM and the model's prediction) and correlate this measure with participant's age in months. Pearson's r with significance level of $p < .05$ will be used for this correlation. If children learn numerals by mapping symbols to their analog counterparts but then replace these relationships with symbol-symbol associations, then we may expect differences in model fit measures across ages. Ratio may fit the neural representation during the first years, but then frequency may become more important. In that case, we should see a negative correlation between model fit measures of the Ratio model and age, but a positive correlation between Frequency model fit and age. For any non-significant correlations with age I will then run a Bayesian Pearson's correlation. Evidence for the null will be estimated using Bayes Factor. Interpretation of the Bayes Factor will be done using the guidelines described above.

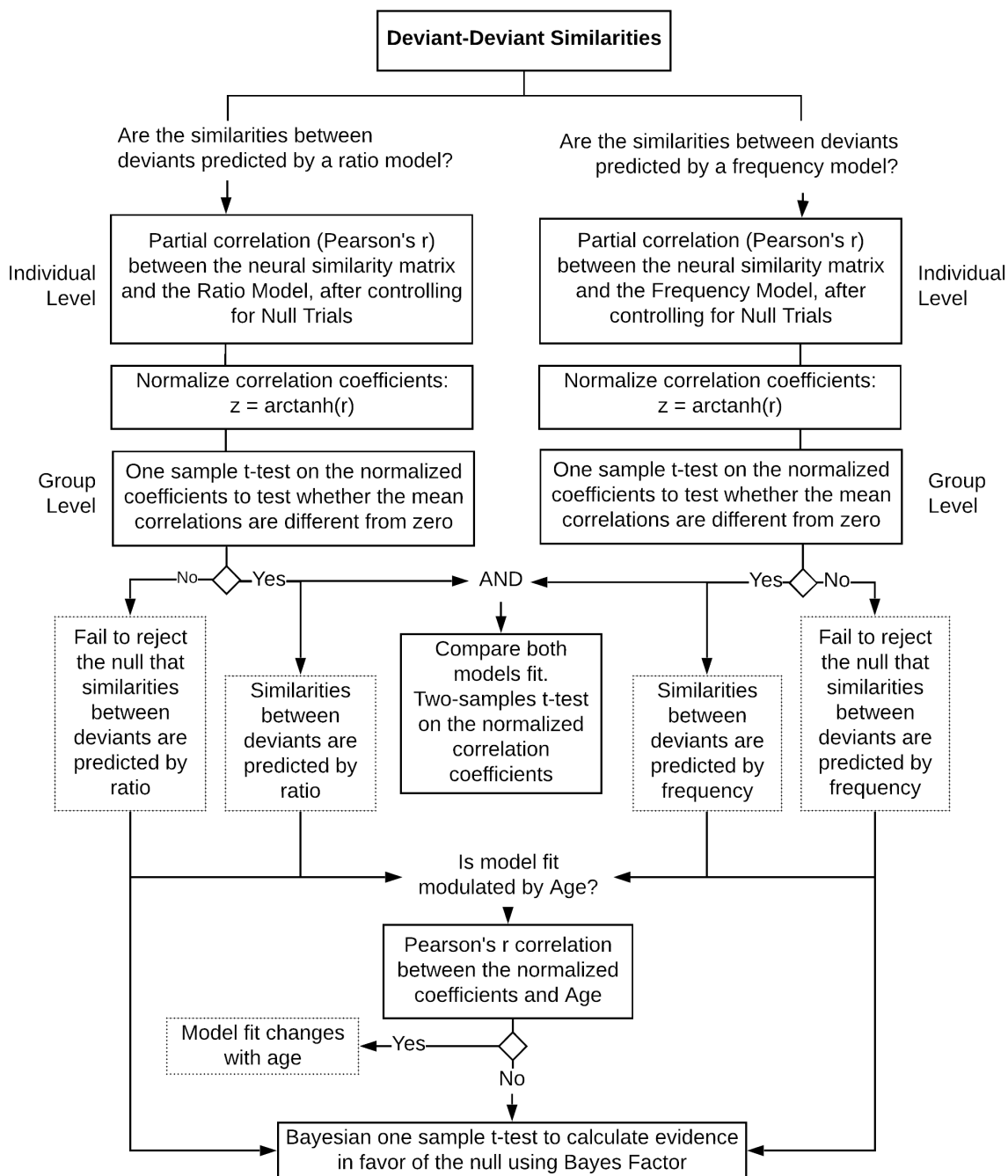


Figure 7. Deviant – Deviant similarity analysis plan

3. Results

3.1. Regions of Interest definition

The conjunction [Main Effect > Baseline] + [Parametric Effect + Baseline] revealed 9 significant clusters showing a meaningful response to the numerical deviants (Table 1, Regions from Univariate contrast). These are regions that respond to the presentation of deviants with an increase in the overall level of activation; but most importantly, the rebound is larger as the deviant was further away from the adaptation numeral. We found significant clusters along bilateral parietal cortex, bilateral fusiform cortex, and others (Figure 8).

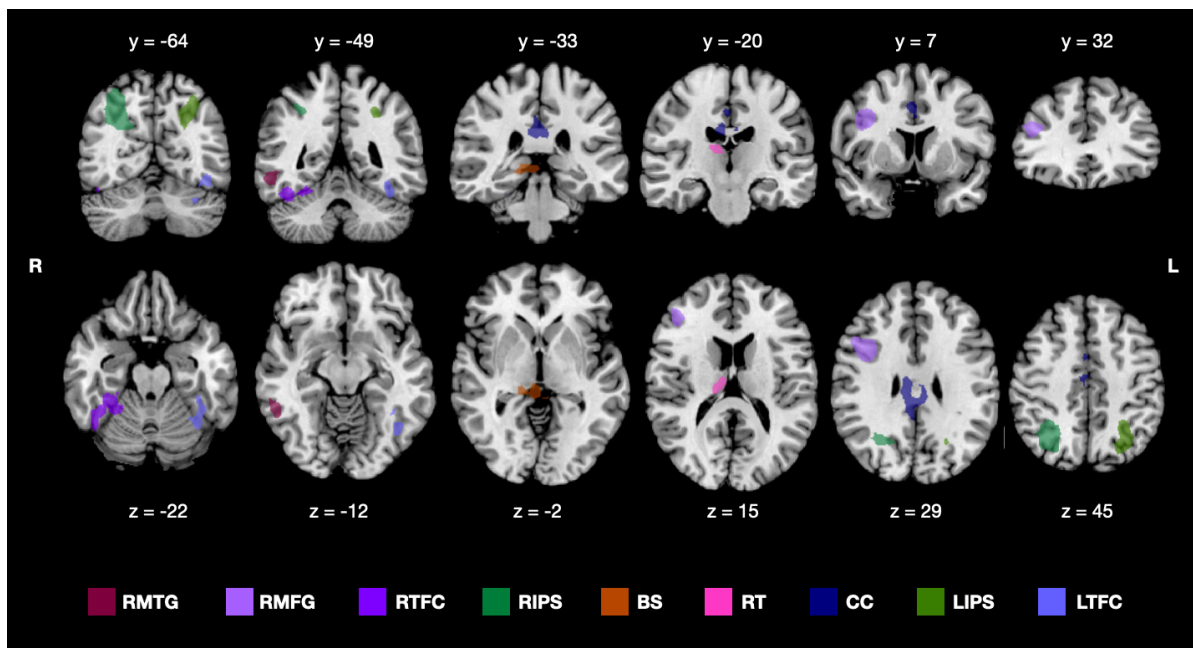


Figure 8. Significant clusters for the univariate contrast [Main > Baseline] + [Parametric > Baseline]. Coordinates are in MNI space.

Table 1. Regions identified with the univariate contrast [Main > Baseline] + [Parametric > Baseline]

ROI Label	Mean x	Mean y	Mean z	SD x	SD y	SD z	Anat. Voxels	Funct. Voxels
Right Middle Temporal Gyrus (RMTG)	55.96	-48.09	-10.41	2.79	3.56	2.83	967	33
Right Middle Frontal Gyrus (RMFG)	42.20	19.96	25.14	4.93	11.86	5.80	6492	261
Right Temporal Fusiform Cortex (RTFC)	36.52	-47.79	-22.55	7.24	6.42	2.55	2452	98
Right Intraparietal Sulcus (RIPS)	30.73	-61.47	43.04	4.58	5.49	7.38	7827	296
Brain Stem (BS)	6.21	-33.39	-3.68	7.29	4.00	2.70	1207	40
Right Thalamus (RT)	9.98	-18.17	12.86	2.99	3.74	2.05	719	27
Cingulate Gyrus (CC)	2.80	-22.41	32.2	4.09	14.81	6.72	4598	193
Left Intraparietal Sulcus (LIPS)	-27.99	-62.14	42.59	3.66	6.20	5.49	4371	167
Right Temporal Fusiform Cortex (RTFC)	-38.52	-55.20	-20.27	3.92	8.49	5.76	2843	125

Coordinates are in MNI space. Number of voxels are provided in both the anatomical and functional space.

Figure 9 shows the regions defined from the probabilistic maps included in the Juelich Atlas. Anatomical information about these clusters, including location and resulting number of voxels after applying the $p > .40$ threshold. Can be found in Table 2

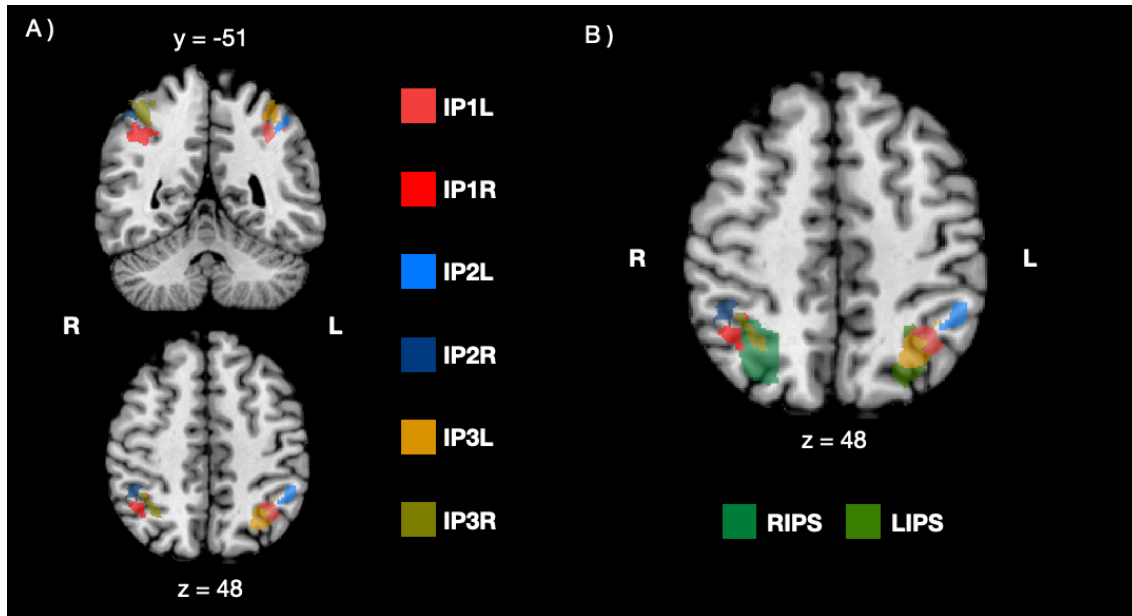


Figure 9. A. Clusters defined from the IPS subdivisions on Juelich Atlas, including only voxels with $p > .40$; B. Comparison of IPS subdivisions and parietal regions from univariate contrast. Coordinates are in MNI space.

Table 2. Regions defined from the probabilistic maps on Juelich Atlas

ROI Label	Mean x	Mean y	Mean z	SD x	SD y	SD z	Anat. Voxels	Funct. Voxels
AIPS_IP1_Left (IP1L)	-36.59	-54.73	44.10	3.67	4.47	4.33	1092	68
AIPS_IP1_Right (IP1R)	40.28	-52.38	43.02	3.91	3.19	3.39	1498	57
AIPS_IP2_Left (IP2L)	-46.7	-45.89	46.25	3.11	3.11	4.33	1030	41
AIPS_IP2_Right (IP2R)	44.39	-45.37	49.49	3.07	3.07	4.88	987	36
AIPS_IP3_Left (IP3L)	-31.79	-60.06	50.00	4.86	4.86	5.74	2380	89
AIPS_IP3_Right (IP3R)	35.04	-55.35	54.92	5.26	5.26	4.99	1964	73

Coordinates are in MNI space. Number of voxels are provided in both the anatomical and functional space.

3.2. Deviant - Adaptation similarities

We performed a repeated measures ANOVA to assess whether the parametric effect observed across the 9 clusters identified from the univariate contrast translated into parametric differences in the distributed patterns of activation. We are reporting significant results at both the uncorrected and corrected thresholds (Table 2), however, for the discussion we will only focus on those effects that remained significant after the correction for multiple comparisons.

We first analyzed the significance of the overall ANOVA model to determine if there was at least one deviant that was significantly more or less similar to the adaptation numeral, compared to the other deviants (see Appendix A for the full ANOVA table). However, for our analysis, the most critical results are the within-subject contrasts (Table 2). This test would tell us whether, at the individual level, the similarities between each deviant and the adaptation numeral follow the trend predicted by ratio or frequency. Regions showing ratio-dependent similarities should have a significant quadratic trend, and regions showing frequency-dependent similarities should have a significant linear trend. The trends observed on each ROI are depicted in Figure 10.

Among the regions defined from the univariate contrast, the overall F for differences across the deviant factor was significant at the uncorrected threshold only in the LIPS cluster ($F(5,220) = 2.26, p = .049, \eta^2 = .049$). In other words, after individual differences in overall similarity values are taken into account, only a 4.9% of the variance in the similarity values was due to differences across deviants. The test of polynomial contrast revealed small but significant linear ($F(1,44) = 4.936, p = .031, \eta^2 =$

.101) and quadratic trends ($F(1,44) = 4.3, p = .044, \eta^2 = .089$) in this region. However, neither the main effect, nor the linear or quadratic trend survived the Dunn-Sidak correction for multiple comparisons.

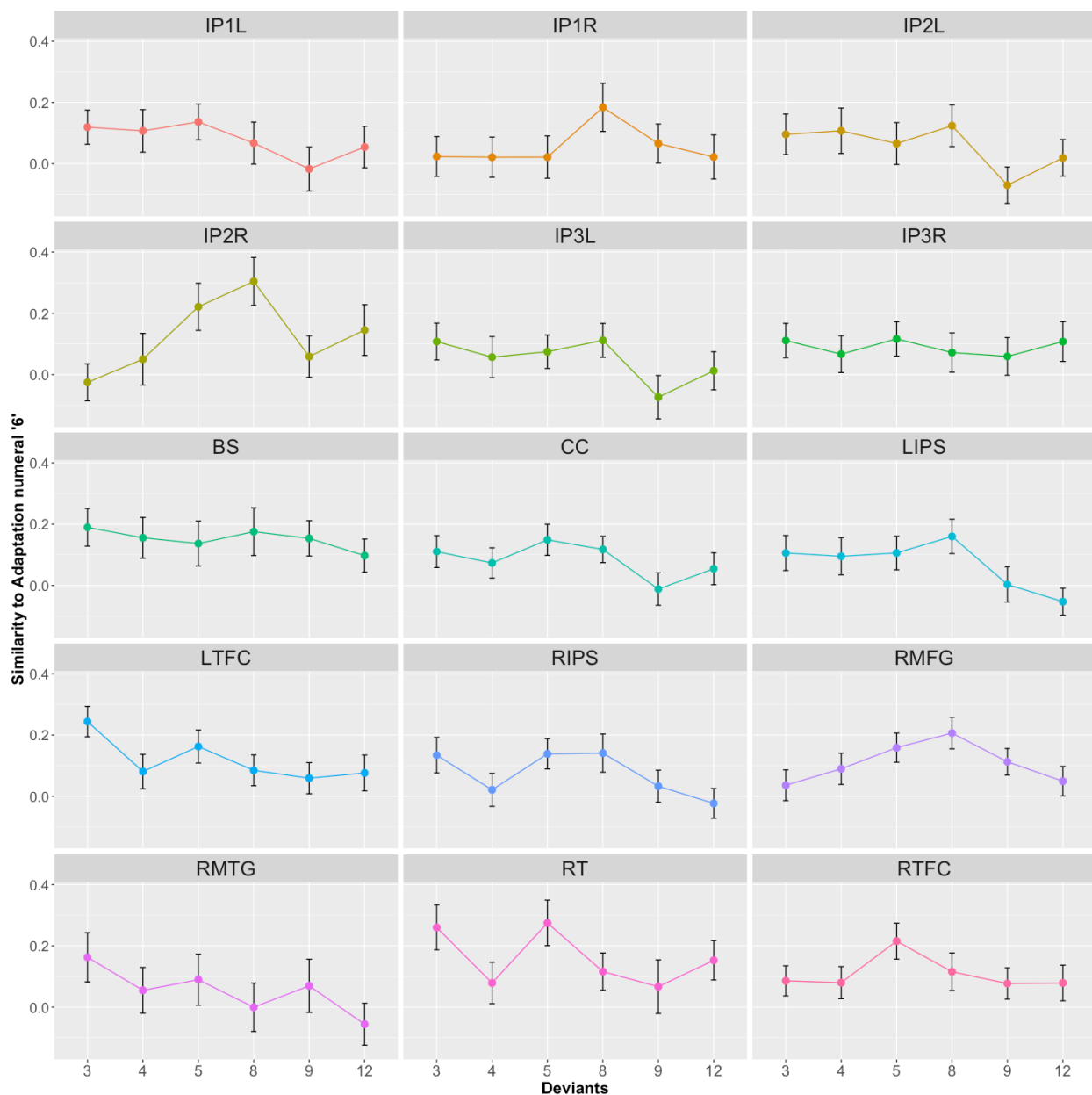


Figure 10. Average similarities between each deviant and the adaptation numeral on each ROI included in the analysis

Table 3. Within-Subject polynomial contrasts of repeated measures.

ROI	CONTRAST	SS	MS	F	Sig.	η^2
IP1L	Linear	0.378	0.378	2.461	0.124	0.053
	Quadratic	0.001	0.001	0.004	0.948	0.000
IP1R	Linear	0.054	0.054	0.339	0.563	0.008
	Quadratic	0.249	0.249	1.621	0.210	0.036
IP2L	Linear	0.474	0.474	3.573	0.065	0.075
	Quadratic	0.026	0.026	0.128	0.722	0.003
IP2R	Linear	0.596	0.596	2.901	0.096	0.062
	Quadratic	1.391	1.391	5.000*	0.030	0.102
IP3L	Linear	0.445	0.445	2.707	0.107	0.058
	Quadratic	0.009	0.009	0.076	0.784	0.002
IP3R	Linear	0.004	0.004	0.043	0.838	0.001
	Quadratic	0.025	0.025	0.143	0.707	0.003
BS	Linear	0.118	0.118	0.759	0.388	0.017
	Quadratic	0.008	0.008	0.041	0.840	0.001
CC	Linear	0.206	0.206	2.093	0.155	0.045
	Quadratic	0.049	0.049	0.421	0.520	0.009
LIPS	Linear	0.664	0.664	4.936*	0.031	0.101
	Quadratic	0.431	0.431	4.300*	0.044	0.089
LTFC	Linear	0.62	0.620	5.198*	0.028	0.106
	Quadratic	0.119	0.119	1.356	0.251	0.030
RIPS	Linear	0.361	0.361	2.93	0.094	0.062
	Quadratic	0.203	0.203	1.974	0.167	0.043
RMFG	Linear	0.021	0.021	0.221	0.640	0.005
	Quadratic	0.82	0.820	8.995**	0.004	0.170
RMTG	Linear	0.834	0.834	3.661	0.062	0.077
	Quadratic	0.002	0.002	0.007	0.935	0.000
RT	Linear	0.344	0.344	2.055	0.159	0.045
	Quadratic	0.068	0.068	0.335	0.566	0.008
RTFC	Linear	0.013	0.013	0.14	0.710	0.003
	Quadratic	0.231	0.231	2.771	0.103	0.059

* Significant at the uncorrected $p < .05$

** Significant Dunn-Sidak correction; this correction was applied separately for each ROI selection method. For ROIs selected from univariate contrast the corrected threshold was $p < .00568$; for the ROIs selected from probabilistic maps the corrected threshold was $p < .00851$

There were other two regions showing significant trends at the within-subject level, even though the overall ANOVA model was not significant. Namely, there was a linear trend in the LTFC cluster ($F(1,44) = 5.198, p = .028, \eta^2 = .106$) that was significant at the uncorrected p-value, but did not survive the multiple comparisons correction. More importantly, there was a quadratic trend in the RMFG cluster ($F(1,44) = 8.995, p = .004, \eta^2 = .17$) which remained significant even after the Dunn-Sidak correction.

The same analysis was done for regions identified from the probabilistic maps. The overall ANOVA model was only significant at the uncorrected threshold in the cluster corresponding to the right IP2 subdivision ($F(5,220) = 2.574, p = .028, \eta^2 = .055$). This means that only 5.5% of the variance in the similarity values was related to differences across deviants, after controlling for individual differences across subjects. This region also showed a quadratic trend ($F(1,44) = 5.0, p = .03, \eta^2 = .102$) that was significant at the uncorrected, but not the corrected threshold.

In summary, for most of our ROI, we failed to find enough evidence to reject the null hypothesis that the mean similarities between each deviant and the adaptation numeral are equal; at least after correcting for multiple comparisons. Only the right Medial Frontal Gyrus showed a significant quadratic trend that survived the correction. These results indicate that, in this region, those deviants that were numerically closer (larger ratio) to the adaptation numeral had more similar distributed patterns of activation than those that are further away.

Two alternative versions of the analysis were also run. First, the analysis was repeated excluding Deviant 12. This is the only two-digit numeral included in the task

and it is also the only one for which Benford's law may not accurately describe its frequency. Additionally, the same model was run but using the zero-order correlations to estimate similarity between the neural patterns, instead of the partial correlations controlling for catch trials reported above. Similar results were obtained on both cases (see Appendix B and C).

3.2.1. *Effect of Age on the Deviant-Adaptation similarities*

In order to test whether there were age-related changes in the structure of similarities between deviants and the adaptation numeral, we added participants age in years as a between-subject factor. Ratio or frequency dependent similarities may be masked at the whole group level and only be evident after accounting for age differences. However, for most regions, we did not find significant interaction between the linear or quadratic contrasts and age (Table 3). Only the BS cluster had an interaction ($F(8,36) = 2.542, p = .026, \eta^2 = .361$), but this was only significant at the uncorrected threshold.

None of these results changed substantially after excluding the deviant "12" was excluded from the analysis or after using zero-order correlations to estimate the similarities, instead of the partial correlations controlling for catch trials reported here (see Appendix D and E).

Table 4. Within-Subject polynomial contrasts: interaction with Age.

ROI	Contrast	SS	MS	F	Sig.	η^2
IP1L	Linear	0.378	0.378	0.834	0.579	0.156
	Quadratic	0.001	0.001	0.531	0.825	0.106
IP1R	Linear	0.054	0.054	1.388	0.235	0.236
	Quadratic	0.249	0.249	0.107	0.999	0.023
IP2L	Linear	0.474	0.474	1.566	0.17	0.258
	Quadratic	0.026	0.026	0.257	0.976	0.054
IP2R	Linear	0.596	0.596	1.331	0.26	0.228
	Quadratic	1.391	1.391	1.973	0.079	0.305
IP3L	Linear	0.445	0.445	0.245	0.979	0.052
	Quadratic	0.009	0.009	1.043	0.423	0.188
IP3R	Linear	0.004	0.004	1.528	0.182	0.254
	Quadratic	0.025	0.025	1.408	0.226	0.238
BS	Linear	0.118	0.118	2.542*	0.026	0.361
	Quadratic	0.008	0.008	0.669	0.715	0.129
CC	Linear	0.206	0.206	1.021	0.438	0.185
	Quadratic	0.049	0.049	1.642	0.147	0.267
LIPS	Linear	0.664	0.664	0.769	0.632	0.146
	Quadratic	0.431	0.431	0.999	0.454	0.182
LTFC	Linear	0.62	0.62	1.631	0.150	0.266
	Quadratic	0.119	0.119	0.401	0.913	0.082
RIPS	Linear	0.361	0.361	1.523	0.184	0.253
	Quadratic	0.203	0.203	0.842	0.573	0.158
RMFG	Linear	0.021	0.021	0.9	0.527	0.167
	Quadratic	0.82	0.82	1.452	0.209	0.244
RMTG	Linear	0.834	0.834	0.724	0.669	0.139
	Quadratic	0.002	0.002	0.539	0.819	0.107
RT	Linear	0.344	0.344	0.987	0.462	0.18
	Quadratic	0.068	0.068	0.262	0.974	0.055
RTFC	Linear	0.013	0.013	0.463	0.874	0.093
	Quadratic	0.231	0.231	1.081	0.398	0.194

* Significant at the uncorrected $p < .05$

** Significant Dunn-Sidak correction; this correction was applied separately for each ROI selection method. For ROIs selected from univariate contrast the corrected threshold was $p < .00568$; for the ROIs selected from probabilistic maps the corrected threshold was $p < .00851$.

3.3. Deviant – Deviant Similarities

We tested whether the correlational structure between the six deviants presented in the task (Figure 11) could be predicted by a Ratio or a Frequency model. We first assessed the similarities between the correlational geometry of the neural representations and the predictions from the model and then tested whether these similarities were significantly different from zero. Our results do not provide evidence in favor of any of these models. The model fit was not significantly different from zero in any of the regions included in the analysis (Table 4). We then used Bayes Factor to calculate the amount of evidence for the null hypothesis. In most cases, the Bayes Factor indicates substantial support for the null hypothesis that the correlations between the model and the data was not significantly different from zero.

Table 5. Ratio and Frequency model fit.

ROI	Ratio Model Fit				Frequency Model Fit			
	t	p	d	BF ₀₁	t	p	d	BF ₀₁
IP1L	1.248	0.219	0.186	2.996	0.260	0.796	0.039	5.994 [†]
IP1R	-1.066	0.292	-0.159	3.636	-1.195	0.239	-0.178	3.181 [†]
IP2L	-0.195	0.846	-0.029	6.078 [†]	1.793	0.080	0.267	1.422
IP2R	-1.261	0.214	-0.188	2.953	-0.224	0.824	-0.033	6.043 [†]
IP3L	-0.729	0.470	-0.109	4.818 [†]	-0.486	0.629	-0.073	5.534 [†]
IP3R	-1.853	0.071	-0.276	1.290	-1.139	0.261	-0.170	3.377 [†]
BS	0.051	0.960	0.008	6.181 [†]	1.101	0.277	0.164	3.511 [†]
CC	0.029	0.977	0.004	6.186 [†]	-1.154	0.255	-0.172	3.324 [†]
LIPS	-0.045	0.964	-0.007	6.183 [†]	-0.836	0.408	-0.125	4.457 [†]
LTFC	-0.419	0.677	-0.062	5.697 [†]	0.789	0.434	0.118	4.617 [†]
RIPS	-0.380	0.705	-0.057	5.779 [†]	-1.167	0.250	-0.174	3.279 [†]
RMFG	-0.647	0.521	-0.097	5.079 [†]	-0.997	0.324	-0.149	3.885 [†]
RMTG	-0.585	0.561	-0.087	5.265 [†]	-1.284	0.206	-0.191	2.873
RT	-0.749	0.458	-0.112	4.754 [†]	0.408	0.685	0.061	5.720 [†]
RTFC	0.523	0.604	0.078	5.439 [†]	-1.038	0.305	-0.155	3.738 [†]

[†] Bayes Factor indicating substantial support for the null

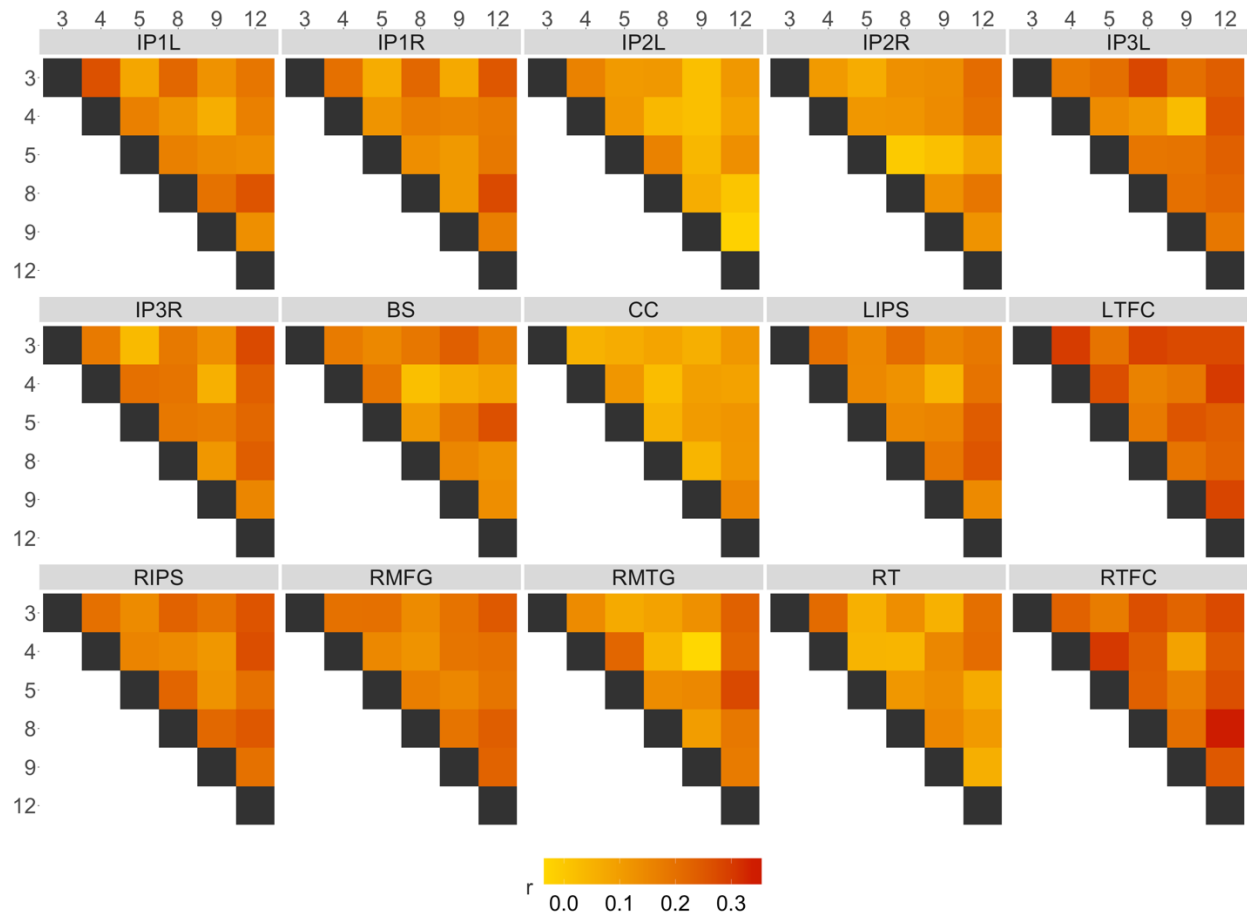


Figure 11. Average Similarity Matrices for each region of interest

We then used a two-samples t-test to compare model fit across both conceptual models (Table 5). We fail to find evidence in favor of any of the models. Moreover, for most of our regions the Bayes Factor indicates substantial support for the null of no difference between the predictive value of both models.

Table 6. Differences between Ratio and Frequency model fit.

ROI	Ratio Model Fit vs. Frequency Model Fit			
	t	p	d	BF
IP1L	0.677	0.500	0.143	4.851 [†]
IP1R	0.256	0.799	0.054	6.024 [†]
IP2L	-1.508	0.135	-0.318	0.788
IP2R	-0.609	0.544	-0.128	5.031 [†]
IP3L	-0.092	0.927	-0.019	6.162 [†]
IP3R	0.117	0.908	0.025	6.155 [†]
BS	-0.846	0.400	-0.178	3.649 [†]
CC	0.832	0.408	0.175	4.749 [†]
LIPS	0.533	0.595	0.112	5.363 [†]
LTFC	-0.873	0.385	-0.184	4.017 [†]
RIPS	0.651	0.517	0.137	5.253 [†]
RMFG	0.485	0.629	0.102	5.598 [†]
RMTG	0.492	0.624	0.104	5.651 [†]
RT	-1.526	0.134	-0.228	2.109
RTFC	0.265	0.792	0.040	5.987 [†]

[†] Bayes Factor indicating substantial support for the null

None of these results changed substantially after excluding the deviant “12” was excluded from the analysis (see Appendix F). Likewise, using zero-order instead of partial correlations yielded similar results (see Appendix G).

3.3.1. Effect of age on the Deviant-Deviant similarities

We assessed whether there were age-related changes in the correspondence between our conceptual models and the observed structure of the neural representation. We used Pearson Correlation to test whether model fit could be predicted from participants age in months (Table 6).

Table 7. Ratio and Frequency model fit correlation with Age.

ROI	Ratio Model Fit ~ Age			Frequency Model Fit ~ Age		
	r	p	BF	r	p	BF
IP1L	0.271	0.072	1.123	-0.193	0.203	2.454
IP1R	0.142	0.353	3.541 [†]	0.116	0.446	4.063 [†]
IP2L	0.143	0.348	3.514 [†]	0.104	0.497	4.305 [†]
IP2R	0.149	0.329	3.390 [†]	-0.056	0.715	5.046 [†]
IP3L	0.157	0.302	3.209 [†]	0.226	0.136	1.837
IP3R	0.459	0.002**	0.041	0.046	0.766	5.157 [†]
BS	0.199	0.191	2.347	-0.029	0.848	5.287 [†]
CC	0.177	0.245	2.796	-0.013	0.934	5.364 [†]
LIPS	0.119	0.436	4.012 [†]	0.117	0.444	4.053 [†]
LTFC	0.447	0.002**	0.055	0.042	0.783	5.189 [†]
RIPS	0.234	0.122	1.685	-0.065	0.670	4.930 [†]
RMFG	0.029	0.853	5.293 [†]	0.221	0.145	1.920
RMTG	0.277	0.066	1.042	-0.168	0.269	2.976
RT	0.492	0.001**	0.018	0.009	0.955	5.374 [†]
RTFC	0.171	0.262	2.924	-0.200	0.187	2.312

* Significant at the uncorrected $p < .05$

** Significant Dunn-Sidak correction; this correction was applied separately for each ROI selection method. For ROIs selected from univariate contrast the corrected threshold was $p < .00568$; for the ROIs selected from probabilistic maps the corrected threshold was $p < .00851$

We found significant positive associations between age and the Ratio model fit on three of our regions. These correlations remained significant after correcting the p value for multiple comparisons. In the IP3R subregion from Juelich Atlas ($r(43) = .459$, $p = .002$, $r^2 = 0.211$), the similarity matrix built from the Ratio model explained around a 21% of the variance in the similarity values from the neural data. A similar correlation was observed in the LTFC cluster ($r(43) = .447$, $p = .002$, $r^2 = 0.200$), in which around a 20% of the neural similarities were predicted by the model. Finally, a positive correlation was also identified in the RT cluster ($r(43) = .492$, $p = .001$, $r^2 = 0.242$), where the model

explained around the 24% of the variance in the neural similarities. All of these correlations were positive, indicating that model fit was better across these regions as age increased (Figure 12).

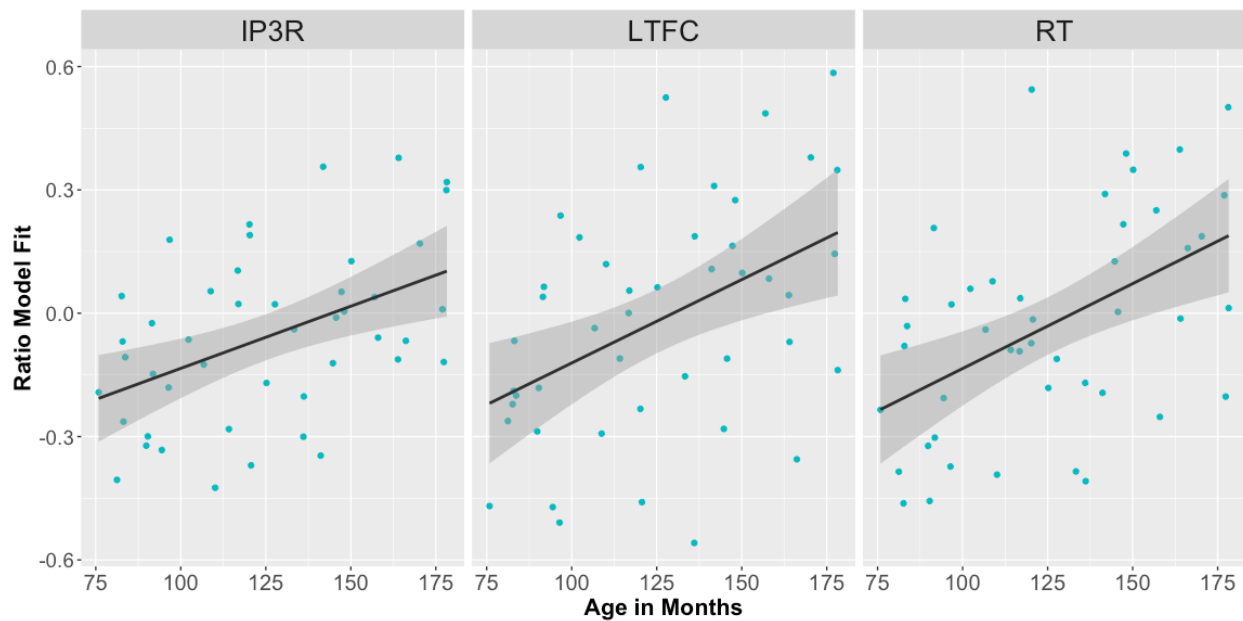


Figure 12. Clusters showing a significant correlation of Ratio Model fit and Age.

Finally, we did not find significant associations between age and the Frequency model fit across any of our ROI. In order to calculate the evidence for the null we performed a Bayesian correlation. Bayes factors indicate substantial support for the null hypothesis that the model fit was not significantly different from zero in most of the regions (Table 6).

None of the correlations changed substantially after excluding the deviant “12” was excluded from the analysis (see Appendix H). Likewise, using zero-order instead of partial correlations yielded similar results (see Appendix I).

4. Discussion

The primary goal of the present thesis was to better characterize, using multivariate neuroimaging analyses, the neural patterns of activation that have been consistently associated with the semantic processing of number symbols (e.g. knowing that 6 is bigger than 9). My second goal was to assess age-related changes in the neural activation patterns. In particular, I was interested in characterizing the spatially distributed neural responses during an fMRI adaptation paradigm in which participants are passively presented with numerals.

In this design there are two stimulus categories: *adaptation numerals* and *deviant numerals*. A train of repeated adaptation numerals (e.g. “6”) is occasionally interrupted by the presentation of deviant numerals (e.g. “8”). The brain response to the deviants are the events of interest in this design. In particular, the repeated presentation of the adaptation numeral is thought to induce a decrease in activation (i.e. adaptation) in regions that code for different aspects of the adaptation numeral; and the presentation of the deviant numerals is thought to lead to a rebound of the overall activation. By manipulating the numerical magnitude of the deviants, researchers have identified regions in which the recovery from habituation varies as a function of the ratio between the deviant and the adaptation numeral (i.e. the response to the deviant increases as the numerical ratio between the adaptation and deviant numeral decreases) (Goffin, 2019; Holloway et al., 2013; Notebaert et al., 2010; Vogel et al., 2015, 2017). Hence, these regions not only seem to detect that a variation has been introduced by the deviant, but also seem to be sensitive to the relative numerical magnitude change. This ratio-dependent parametric effect is most commonly observed in the parietal cortex,

which, convergent with the results of studies in which participants had to actively process the meaning of numerals, suggests that this region has a relevant role in the processing of the numerical magnitude information conveyed by the symbols.

What might explain the presence of such a parametric effect of ratio on brain activation? Against the background of data from single-cell neurophysiology which revealed that there exist neurons that are approximately tuned to specific numbers (Nieder et al., 2002; Nieder & Miller, 2003, 2004), researchers have speculated that the parametric effect reflects a representation of numerals in which numbers close to each other are represented by partially overlapping neuronal populations. For example, Notebaert and colleagues (2010) note that the ratio-dependent parametric recovery from adaptation *“is in line with the idea that symbolic numbers are represented by a place coding system [...]. According to this principle, numbers activate their own corresponding set of neurons and will partially activate the neuronal set of neighboring magnitudes with a decreasing strength as a function of numerical distance”* (Notebaert et al., 2010). This has been the most prominent explanatory account of this fMRI adaptation effect.

However, since univariate analysis are not sensitive to properties of the distributed voxel-by-voxel BOLD response, they are not suited to directly test hypotheses about the degree of overlap/correlation between the populations of neurons coding for different number symbols. As a result, the nature of this effect remains poorly understood. Put differently, the current explanation of the ratio dependent response to the numerical deviants cannot be directly tested using univariate analyses. In the current study, I set out to investigate the relationship between the patterns corresponding to the different

deviants in an effort to better understand whether the similarity space generated during this task fits the aforementioned hypothesis.

Critically, the account of the parametric effect in terms of shared representations directly leads to the prediction of a particular correlational structure of the neural responses to deviant numbers. Namely, the pattern of activation elicited by numerals that are closer in magnitude should be more similar than those of numerals that are further away. In this way, the Ratio model assumes that the representation of numbers is organized according to the magnitudes they represent.

In addition, motivated by recent theories arguing that there are other associations among symbols that are perhaps more relevant than the magnitudes they represent, I also set out to test an alternative model which predicts that the representation of the numerals is organized according to their relative frequency. More specifically, recent studies have revealed that the frequency with which two numerals co-occur in the world can account for ratio signatures in behavioral performance (Krajcsi et al., 2016). More importantly, there is recent evidence that this frequency model accurately describes similarities in the neural patterns of activation associated with numerals (Lyons & Beilock, 2018). In summary, in the present thesis, using RSA analysis, I sought to investigate whether fMRI adaptation data can be statistically predicted by a ratio-dependent or a frequency dependent model.

4.1. Predictive value of the Ratio Model

Contrary to the most prominent account of univariate ratio-dependent recovery from numeral adaptation data, my RSA analysis does not offer support for a correlational structure between numerals that depends on the ratio between the

adaptation numeral and the deviant. The lack of evidence in favor of the ratio model is particularly remarkable for those regions defined from the univariate contrast. Specifically, these regions were selected because they exhibited significant ratio-dependent increases in activation at the univariate level. Said differently, the differences in the mean activation of these regions in response to deviant numerals did not translate into the predicted similarity structure of the distributed patterns. These results were further confirmed by the analysis of similarities among deviants alone. We found that the Ratio model was not a good predictor of the correlational geometry of the neural patterns associated with the deviants. Moreover, for most of the regions, Bayesian analysis revealed there was substantial evidence in favor of the null hypothesis that the correlation between the Ratio model and the neural data was not significantly different from zero. In some cases, the null was up to 5 times more likely than the alternative hypothesis, given the data observed.

Our results are in line with findings from previous RSA analyses of numerical processing (Lyons et al., 2015b; Lyons & Beilock, 2018). These authors also found no ratio-dependent correlational structure of the fMRI response to numerals during a matching task. Our results and Lyons et al's do not support the previously held notion that symbolic numerals are represented by an imprecise system of numerosity selective neurons with overlapping responses. Under this view, the amount of overlap in the neuronal population code that is used to represent any two numerals is determined by their ratio: as the ratio gets closer to one, the overlap in the representation is more pronounced, which explains why these numerals harder to discriminate during behavioral tasks.

Put differently, our findings show that numeral 6 was as similar to numeral 3 as it was to numeral 8. This was confirmed by our ANOVA results showing that, in most regions, the similarities between each of the deviants and the adaptation numeral were equivalent (Figure 10). In addition, by looking at our average similarity matrices (Figure 11) it is also apparent, for a given region, there was very low variabilities in the correlations between the deviants. More indirectly, our findings are also consistent with the study by Harvey et al (2013) who identified regions having a topographic organization of the representation of non-symbolic magnitudes, but not for number symbols.

4.2. Predictive value of the Frequency Model

Across all of our analyses, we failed to find evidence of frequency-dependent similarities in the patterns associated with numerals. Furthermore, on 13 out the 15 regions included in the analysis, we found substantial evidence for the null hypothesis that the frequency model fit was not significantly different from zero. These results are in contrast with findings reported by Lyons et al. (2018). They found evidence to suggest that the organization of symbolic numerals in the adult brain can be predicted by symbol-symbol association, which are determined by the frequency of co-occurrence of numerals. Our results do not converge with this account.

It is possible that the lack of convergence of the results reported in this thesis and those reported by Lyons et al's (2018) is due to differences between the children data analyzed here and adult data analyzed by them. We know from the frequency calculations reported by Dehaene and Mehler (1992) that Benford's Law accurately

describes the frequency of spontaneous occurrence of numerals in everyday life.

Therefore, it is reasonable that the patterns observed in the neural organization of the adult brain reflects these biases. However, in the case of children, “everyday life” interactions with numerals occur in the more controlled context of school. As a result, semantic associations between number symbols may be strongly biased in children by a different set of factors, like multiplication tables and other number facts, whose influence is less strong in adults. The model tested in this study may not accurately reflect these specific biases.

For example, calculating the frequency of co-occurrence of two numerals by multiplying their individual probabilities assumes that these probabilities are independent. If children symbol-symbol associations are mediated, for example, by the frequency with which they appear together in multiplication facts, this independence is not granted. In fact, we know from studies estimating the frequency of number facts in math books from 1st to 6th grade that 2X multiplication facts are up to twice more frequent than 9X facts (Ashcraft & Christy, 1995). This would result in numerals like 6 and 12 occurring more frequently together (as in “2 times 6 equals 12”) than, for example, 6 and 8 (as in “6 times 8 equals 48”), in contrast to what our model predicts. In essence, it is possible that symbol-symbol associations are more prominent than symbol-magnitude in the children's brain, just like has been described in adults. However, in order to model them appropriately, we need to develop more specific models of these associations that take into account the particular biases determined by interactions with numbers in the school context.

Another difference between our study and Lyon et al's has to do with the nature of the task. They measured the pattern of brain activity during a matching task using number symbols. Participants were presented with a numeral and had to decide whether the following numeral was equal or different. In contrast, during our task, participants were not required to do any sort of numerical judgement (they only had to press a button when a Smurf appeared on the screen). It is possible that semantic associations among numerals are only activated if they are relevant for the task, which may explain why such relationships are not evident during our passive design.

4.3. Age related effects

Another important question I addressed, in the present thesis, is whether the lack of evidence for both of these models at the group level can be explained by age-related changes in their fits to the data. Put differently, it is possible that the relative fit of the two models undergoes age-related changes. Previous univariate analysis of this dataset failed to find correlations between age and the parametric effect (Goffin, 2019). In contrast, we did find age related changes in the predictive value of the Ratio model in 3 out of the 15 regions of interest, including one of the subdivisions of the Intraparietal Sulcus located in the right hemisphere (IP3R). As age increased, the organizational structure of the representation in this region was progressively more similar to the pattern predicted by the ratio model: numerals that are closer have more similar representation than the ones that are further away. These trends remained significant after correcting for multiple comparison.

As has been mentioned before, taking all of our regions together, our analysis does not favor the existence of associations among numerals on the base of their relative magnitude differences, as predicted by the Ratio model. Nevertheless, the observed age-related increases in model fit along specific clusters may suggest that this type of representation emerges in parietal cortex over developmental time. Previous studies describing developmental changes in the neural circuits involved in numerical processing have found differences in the recruitment of both frontal and parietal regions in children vs adults (Ansari et al., 2005b). Compared to adults, children seem to rely more in frontal networks during numerical tasks and it is only later in development that parietal networks become engaged. Interestingly, this developmental shift from frontal to parietal cortex is also consistent with another result from this study. The only area showing a pattern of similarities consistent with the Ratio across the whole group is a cluster in the Middle Frontal Gyrus. It is possible that we were able to find magnitude-dependent similarities only in these frontal regions just because they are more involved in the processing of symbolic stimuli in children. If parietal areas, on the other hand, are recruited later in development, activation across these regions may be noisier in younger children.

Correlations between Age and the Ratio model fit was also present on the left temporal fusiform cortex. This region has been consistently identified by previous studies that tested for ratio-dependent recovery from adaptation (Holloway et al., 2013; Vogel et al., 2017). However, unlike the parietal cortex, left fusiform regions are considered to be involved in the processing of visual features of the numerals. For example, Holloway et al. (2013), found that this was the only region showing a recovery

from activation consistent with a model based on shared visual features among the numerals. However, further follow up analysis have suggested that processing in this region is more complex than previously thought. Namely, Vogel et al. (2017) used a variation of the adaptation paradigm in which numerals were presented either visually or aurally and found that parametric effects in the left fusiform gyrus also appear in the auditory condition. The authors argue that activation in this region may not be purely visual. Instead, it seems to be influenced by top-down modulation from other regions that are engaged in the processing of the semantic meaning of numerals. In summary, the factors that explain the parametric recovery of activation in response to deviants on fusiform cortex are still unclear. Notably, none of these previous studies has analyzed the pattern information that underlie the aforementioned effects, which can help to elucidate how much of this response reflects the coding of numerical or visual features. Our data predicts that, at least in the adult brain, ratio-dependent similarities should be expected in the pattern of activation associated with the presentation of numerals in this region. It is possible that the fusiform cortex is involved in the association of the visual shape of the symbol and its meaning (Grotheer et al., 2018; Yeo et al., 2017), which would explain why both visual and semantic effects are observed in this region. This hypothesis would be in line with our results, since it is possible that such associations become stronger as children have increasingly more experience with numerals, which may result in the age-modulation of the ratio model observed here.

4.4. Adaptation vs. Multivariate analysis

One of the most striking result of the present thesis is the strong lack of convergence between the univariate responses and the multivariate similarity analysis of the data. It is true that these two methods are sensitive to different properties of the neural data and thus, conclusions from one and the other do not need to completely match. Univariate analysis of fMRI data capture differences in the overall activation of brain regions in response to stimuli and do not consider voxel-by-voxel differences (indeed these are reduced by the use of spatial smoothing of the data). Multivariate analyses, on the other hand, are more sensitive to fine-grained information in the patterns of activation. Most reports comparing the two methods highlight that multi-voxel patterns are usually more sensitive to detect selectivity of the underlying neuronal populations than adaptation paradigms (Sapountzis et al., 2010). The pattern observed in our data is rather different. We have adaptation data suggesting a particular structure of the representation, which is not supported by the multivariate methods.

These results raise the question of whether the parametric effect is actually being driven by numerical selectivity along neurons of these regions. Recent reviews of the adaptation literature highlight that adaptation effects do not necessarily reflect selectivity of the underlying populations of neurons (Larsson et al., 2016). Other factors like attention or differences in neurovascular coupling may also account for these effects. Yet, we have evidence to believe there is a numerical component of this effect, especially in the parietal cortex. Using a cross-linguistic version of this paradigm, Holloway et al. (2013) compared participants' responses when presented with Hindu-Arabic numerals and Chinese characters. They found that parametric recovery from

adaptation only occurs when participants know the meaning of the symbols that are being presented, suggesting that this effect is driven by a semantic processing of the numerals and not just low-level properties of the stimuli. Another study by Goffin et al. (2019) tested whether ordinal relations could explain the parametric recovery by presenting participants with both letters and numbers (both are ordered sequences). They found that, in contrast to numbers, letters do not induce parametric recovery from adaptation in any region of the brain.

However, it is possible that this numerical component is heavily mixed with other task-related effects such as motor response. Despite the very low demands of this task, it is certainly not completely passive. Participants are instructed to press a button when a certain stimulus appears on the screen. These occasional button presses appear in the context of a paradigm in which participants mostly see the same stimulus (i.e the adaptation numeral). Therefore, when a change is introduced in the form of a number deviant, a motor response may need to be inhibited. In fact, the parietal cortex is considered to be part of the dorsal stream, a network thought to be involved in perceptual processing of action-relevant stimuli (Goodale & Milner, 1992). Moreover, recent studies have shown that action-related activation occurs in parietal regions even when no explicit action is required (for a review see Culham & Valyear, 2006). It is possible that the activation we see in these regions is the result of a mixed effect of a motor and a numerical component. In fact, it may be the case that the amount to which the activation reflects the processing of the numerical magnitude of the deviant numerals is relatively small and, as a result, there is not consistent evidence for numerical relationships in the multivariate patterns.

It is also possible that the experimental design employed here, which was optimized to find differences in the habituation response, is simply not suited for obtaining accurate and reliable multi-voxel pattern information. One recent study suggests that multivariate pattern analysis techniques are particularly sensitive to variability in the estimates of the beta weights corresponding to each experimental condition (Davis et al., 2014). The passive nature of the task and its corresponding low attentional demands may result in a very large inter-trial variability in the patterns associated with the numerals. This, combined with the limited number trials available for each condition during our task, may difficult the accurate estimation of the beta weights, rendering the MVPA analysis inaccurate.

4.5. Implications for future studies

Adaptation studies like the one reported in this thesis have been largely used as an alternative to avoid confounds in the neural activation that are due to task demands and response selection. Our study reveals that future studies wanting to take advantage of this paradigm should also consider complementing univariate contrasts with analysis of the underlying pattern information. Specifically, future studies may benefit from using whole-brain pattern analysis, such as a combination of RSA with a searchlight approach, in order to identify regions showing patterns of similarities consistent with relevant conceptual models that may not have been evident at the univariate level.

More broadly, our study tested predictions from a theory that has been very influential in the field of numerical cognition, suggesting that the neural code used to represent numerals is imprecise and characterized with increasing overlap between the

representations as the numerals are numerically closer. Our data does not offer support for such ratio-dependent imprecision in the way numerals are coded in the brain. However, further studies are necessary to test some of the alternative theories that have been proposed. For example, some authors suggest that association between symbols and their magnitude are necessary to understand the meaning of the first learned symbols (e.g. 1, 2 and 3). Even though semantic association are more relevant for later stages of learning involving larger numbers, ratio-dependent associations may still persist for the smaller numerals (Reynvoet & Sasanguie, 2016). Our study cannot directly address this possibility given the limited number of stimuli included in this dataset. Future studies would benefit from using more stimuli-rich designs than the one presented here.

Finally, one important follow up to this study would be to use the same analysis described here in a dataset from adult participants. The associations we found between the ratio model fit and age lead to predictions regarding some regions of the brain where the ratio model should fit the adult neural data. However, this prediction is contrary to other studies using RSA on data from active tasks, which have failed to find such ratio-dependent patterns in adults (Lyons et al., 2015b; Lyons & Beilock, 2018). Further studies are needed to address whether such ratio-dependent similarities are task-dependent.

5. Conclusions

The notion that numerical symbols are coded in the brain by a system of numerosity selective neurons with overlapping tuning curves has been highly influential in the field of numerical cognition (Dehaene et al., 1998; Piazza et al., 2007). Originally, this theory was put forward as a possible explanation for the ratio effects observed in behavioral number comparison tasks: as the ratio between two numerals is closer to one, participants take more time to compare the numerals and make more mistakes. The tuning curve model assumes that these behavioral effect results from the imprecisions in the neural code used to represent number symbols. This theory has been supported by a large body of neuroimaging research showing ratio-dependent responses in regions of the parietal cortex. Although these results are consistent with the overlapping tuning curve model, they did not offer direct evidence of overlapping patterns of activation in response to numerals. The current study was the first one to directly address this assumption from adaptation data by testing whether the similarities in the patterns of activation obtained during the presentation of Hindu-Arabic symbols are modulated by their numerical ratio. In 14 out of the 15 regions analyzed, we failed to find evidence in favor of this ratio-dependent similarities hypothesis. Instead, our results are more consistent with the idea that number symbols are represented as discrete entities, as previous studies have suggested (Krajcsi et al., 2016; Lyons et al., 2015b; Lyons & Beilock, 2018; Reynvoet & Sasanguie, 2016). These null results have relevant implications for our understanding of how numerals are represented in the brain. Our data does not provide evidence of ratio-dependent imprecisions in the neural code used to represent numerals that may explain the ratio effects observed in behavioral tasks.

As a result, we argue that alternative accounts already offered in the literature should be more closely considered.

As part of the present study I actually tested one of those alternative models. Namely, the possibility that this discrete representation of numerals is organized according to the frequency in which numbers occur together in real life. Although this theory has already received support from neuroimaging evidence in the adult brain (Lyons et al., 2015b; Lyons & Beilock, 2018), I failed to find similar results in the current sample from children. Future studies should examine whether the influence of frequency of the numerals upon the organization of the representation is experience-dependent and thus, it is only evident later in development.

Taken together, the results I report in the present thesis challenge previously held notions about the meaning of the neural habituation effects observed during this task. In the light of our limited understanding of the neural processes underlying this effect, we argue that future studies should complement univariate analysis of habituation and signal recovery effects with multivariate approaches.

6. References

- Ansari, D., Garcia, N., Lucas, E., Hamon, K., & Dhital, B. (2005a). Neural correlates of symbolic number processing in children and adults. *NeuroReport*, *16*(16), 1769–1773. <https://doi.org/10.1097/01.wnr.0000183905.23396.f1>
- Ansari, D., Garcia, N., Lucas, E., Hamon, K., & Dhital, B. (2005b). Neural correlates of symbolic number processing in children and adults. *NeuroReport*, *16*(16), 1769–1773. <https://doi.org/10.1097/01.wnr.0000183905.23396.f1>
- Ashcraft, M. H. ., & Christy, K. S. . (1995). The Frequency of Arithmetic Facts in Elementary Texts : Addition and Multiplication in Grades 1-6. *Journal for Research in Mathematics Education*, *26*(5), 396–421.
- Benford, F. (1938). The Law of Anomalous Numbers. *Proceedings of the American Philosophical Society*, *78*(4), 551–572.
- Bulthé, J., De Smedt, B., & Op de Beeck, H. P. (2014). Format-dependent representations of symbolic and non-symbolic numbers in the human cortex as revealed by multi-voxel pattern analyses. *NeuroImage*, *87*, 311–322. <https://doi.org/10.1016/j.neuroimage.2013.10.049>
- Bulthé, J., De Smedt, B., & Op de Beeck, H. P. (2018). Arithmetic skills correlate negatively with the overlap of symbolic and non-symbolic number representations in the brain. *Cortex*, *101*(January), 306–308. <https://doi.org/10.1016/j.cortex.2018.01.008>
- Bulthé, J., Smedt, B. De, & Beeck, H. P. Op de. (2015). Visual number Beats Abstract Numerical Magnitude: Format-Dependent Representation of Arabic Digits and Dot Patterns in the human parietal cortex. *Journal of Cognitive Neuroscience*, 1–33.

- Cantlon, J. F. (2012). Math, monkeys, and the developing brain. *Proceedings of the National Academy of Sciences of the United States of America*, *109*(SUPPL.1), 10725–10732. <https://doi.org/10.1073/pnas.1201893109>
- Cantlon, J. F., & Brannon, E. M. (2006). Shared system for ordering small and large numbers in monkeys and humans. *Psychological Science*, *17*(5), 401–406. <https://doi.org/10.1111/j.1467-9280.2006.01719.x>
- Choi, H. J., Zilles, K., Mohlberg, H., Schleicher, A., Fink, G. R., Armstrong, E., & Amunts, K. (2006). Cytoarchitectonic identification and probabilistic mapping of two distinct areas within the anterior ventral bank of the human intraparietal sulcus. *Journal of Comparative Neurology*, *495*(1), 53–69. <https://doi.org/10.1002/cne.20849>
- Cohen, D. J. (2009). Integers do not automatically activate their quantity representation. *Psychonomic Bulletin and Review*, *16*(2), 332–336. <https://doi.org/10.3758/PBR.16.2.332>
- Culham, J. C., & Valyear, K. F. (2006). Human parietal cortex in action. *Current Opinion in Neurobiology*, *16*(2), 205–212. <https://doi.org/10.1016/j.conb.2006.03.005>
- Damarla, S. R., & Just, M. A. (2013). Decoding the representation of numerical values from brain activation patterns. *Human Brain Mapping*, *34*(10), 2624–2634. <https://doi.org/10.1002/hbm.22087>
- Davis, T., LaRocque, K. F., Mumford, J. A., Norman, K. A., Wagner, A. D., & Poldrack, R. A. (2014). What do differences between multi-voxel and univariate analysis mean? How subject-, voxel-, and trial-level variance impact fMRI analysis. *NeuroImage*, *97*, 271–283. <https://doi.org/10.1016/j.neuroimage.2014.04.037>

- Dehaene, S. (1992). Varieties of numerical abilities. *Cognition*, *42*, 1–42.
[https://doi.org/10.1016/0010-0277\(92\)90049-N](https://doi.org/10.1016/0010-0277(92)90049-N)
- Dehaene, S., Dehaene-Lambertz, G., & Cohen, L. (1998). Abstract representations of numbers in the animal and human brain. *Trends in Neurosciences*, *21*(8), 355–361.
[https://doi.org/10.1016/S0166-2236\(98\)01263-6](https://doi.org/10.1016/S0166-2236(98)01263-6)
- Dehaene, S., Dupoux, E., & Mehler, J. (1990). Is Numerical Comparison Digital? Analogical and Symbolic Effects in Two-Digit Number Comparison. *Journal of Experimental Psychology: Human Perception and Performance*, *16*(3), 626–641.
<https://doi.org/10.1037/0096-1523.16.3.626>
- Dehaene, S., & Mehler, J. (1992). Cross-linguistic regularities in the frequency of number words. *Cognition*, *43*, 1:19.
- Diester, I., & Nieder, A. (2007). Semantic associations between signs and numerical categories in the prefrontal cortex. *PLoS Biology*, *5*(11), 2684–2695.
<https://doi.org/10.1371/journal.pbio.0050294>
- Duncan, E. M., & McFarland, C. E. (1980). Isolating the effects of symbolic distance, and semantic congruity in comparative judgments: An additive-factors analysis. *Memory & Cognition*, *8*(6), 612–622. <https://doi.org/10.3758/BF03213781>
- Eger, E., Michel, V., Thirion, B., Amadon, A., Dehaene, S., & Kleinschmidt, A. (2009). Deciphering Cortical Number Coding from Human Brain Activity Patterns. *Current Biology*, *19*(19), 1608–1615. <https://doi.org/10.1016/j.cub.2009.08.047>
- Eickhoff, S. B., Heim, S., Zilles, K., & Amunts, K. (2006). Testing anatomically specified hypotheses in functional imaging using cytoarchitectonic maps. *NeuroImage*, *32*(2), 570–582. <https://doi.org/10.1016/j.neuroimage.2006.04.204>

- Feigenson, L., Dehaene, S., & Spelke, E. (2004). Core systems of number. *Trends in Cognitive Sciences*, 8(7), 307–314. <https://doi.org/10.1016/j.tics.2004.05.002>
- Forman, S. D., Cohen, J. D., Fitzgerald, M., Eddy, W. F., Mintun, M. A., & Noll, D. C. (1995). Improved Assessment of Significant Activation in Functional Magnetic Resonance Imaging (fMRI): Use of a Cluster-Size Threshold. *Magnetic Resonance in Medicine*, 33(5), 636–647. <https://doi.org/10.1002/mrm.1910330508>
- Gallistel, C. R., & Gelman, R. (1992). Preverbal and verbal counting and computation. *Cognition*, 44, 43–74.
- Goebel, R., Esposito, F., & Formisano, E. (2006). Analysis of FIAC data with BrainVoyager QX : From single - subject to cortically aligned group GLM analysis and self - organizing group ICA. *Human Brain Mapping*, 27(5), 392–401. http://download.brainvoyager.com/doc/Goebel_etal_Preprint_HBM2006.pdf
- Goffin, C. (2019). *How does the brain represent digits ? Investigating the neural correlates of symbolic number representation using fMRI- Adaptation*. University of Western Ontario.
- Goffin, C., Sokolowski, H. M., Slipenkyj, M., & Ansari, D. (2019). Does writing handedness affect neural representation of symbolic number? An fMRI Adaptation Study. *Cortex*, 121, 27–43. <https://doi.org/10.1016/j.cortex.2019.07.017>
- Goodale, M. A., & Milner, A. D. (1992). Separate visual pathways for perception and action. *Trends in Neurosciences*, 15(1), 20–25. [https://doi.org/https://doi.org/10.1016/0166-2236\(92\)90344-8](https://doi.org/https://doi.org/10.1016/0166-2236(92)90344-8)
- Grill-Spector, K. (2006). Selectivity of Adaptation in Single Units: Implications for fMRI Experiments. *Neuron*. <https://doi.org/10.1016/j.neuron.2006.01.004>

- Grill-Spector, K., & Malach, R. (2001). fMR-adaptation: A tool for studying the functional properties of human cortical neurons. *Acta Psychologica*, *107*(1–3), 293–321.
[https://doi.org/10.1016/S0001-6918\(01\)00019-1](https://doi.org/10.1016/S0001-6918(01)00019-1)
- Grotheer, M., Jeska, B., & Grill-Spector, K. (2018). A preference for mathematical processing outweighs the selectivity for Arabic numbers in the inferior temporal gyrus. *NeuroImage*, *175*(November 2017), 188–200.
<https://doi.org/10.1016/j.neuroimage.2018.03.064>
- Halberda, J., & Feigenson, L. (2008). Developmental Change in the Acuity of the “Number Sense”: The Approximate Number System in 3-, 4-, 5-, and 6-Year-Olds and Adults. *Developmental Psychology*, *44*(5), 1457–1465.
<https://doi.org/10.1037/a0012682>
- Holloway, I. D., & Ansari, D. (2009). Mapping numerical magnitudes onto symbols: The numerical distance effect and individual differences in children’s mathematics achievement. *Journal of Experimental Child Psychology*, *103*(1), 17–29.
<https://doi.org/10.1016/j.jecp.2008.04.001>
- Holloway, I. D., & Ansari, D. (2010). Developmental specialization in the right intraparietal sulcus for the abstract representation of numerical magnitude. *Journal of Cognitive Neuroscience*, *22*(11), 2627–2637.
<https://doi.org/10.1162/jocn.2009.21399>
- Holloway, I. D., Battista, C., Vogel, S. E., & Ansari, D. (2013). Semantic and perceptual processing of number symbols: Evidence from a cross-linguistic fMRI adaptation study. *Journal of Cognitive Neuroscience*, *25*(3), 388–400.
https://doi.org/10.1162/jocn_a_00323

- Holloway, I. D., Price, G. R., & Ansari, D. (2010). Common and segregated neural pathways for the processing of symbolic and nonsymbolic numerical magnitude: An fMRI study. *NeuroImage*, *49*(1), 1006–1017.
<https://doi.org/10.1016/j.neuroimage.2009.07.071>
- Jarosz, A. F., & Wiley, J. (2014). What Are the Odds? A Practical Guide to Computing and Reporting Bayes Factors. *Journal of Problem Solving*, *7*, 2–9.
<https://doi.org/10.7771/1932-6246.1167>
- JASP Team. (2019). *JASP (Version 0.10.2)[Computer software]*. <https://jasp-stats.org/>
- Krajcsi, A., Lengyel, G., & Kojouharova, P. (2016). The source of the symbolic numerical distance and size effects. *Frontiers in Psychology*, *7*(NOV), 1–16.
<https://doi.org/10.3389/fpsyg.2016.01795>
- Kriegeskorte, N., Mur, M., & Bandettini, P. (2008). Representational similarity analysis - connecting the branches of systems neuroscience. *Frontiers in Systems Neuroscience*, *2*(NOV), 1–28. <https://doi.org/10.3389/neuro.06.004.2008>
- Kriegeskorte, N., Simmons, W. K., Bellgowan, P. S., & Baker, C. I. (2009). Circular analysis in systems neuroscience: The dangers of double dipping. *Nature Neuroscience*, *12*(5), 535–540. <https://doi.org/10.1038/nn.2303>
- Larsson, J., Solomon, S. G., & Kohn, A. (2016). fMRI adaptation revisited. *Cortex*, *80*, 154–160. <https://doi.org/10.1016/j.cortex.2015.10.026>
- Leibovich, T., & Ansari, D. (2016). The Symbol-Grounding Problem in Numerical Cognition: A Review of Theory, Evidence, and Outstanding Questions. *Canadian Journal of Experimental Psychology*, *70*(1), 12–23.
<https://doi.org/10.1037/cep0000070>

- Leibovich, T., Katzin, N., Harel, M., & Henik, A. (2017). From “sense of number” to “sense of magnitude”: The role of continuous magnitudes in numerical cognition. *Behavioral and Brain Sciences*, 40. <https://doi.org/10.1017/S0140525X16000960>
- Lloyd, S. P. (1982). Least Squares Quantization in PCM. *IEEE Transactions on Information Theory*, 28(2), 129–137. <https://doi.org/10.1109/TIT.1982.1056489>
- Lyons, I. M., Ansari, D., & Beilock, S. L. (2012). Symbolic estrangement: Evidence against a strong association between numerical symbols and the quantities they represent. *Journal of Experimental Psychology: General*, 141(4), 635–641. <https://doi.org/10.1037/a0027248>
- Lyons, I. M., Ansari, D., & Beilock, S. L. (2015a). Qualitatively different coding of symbolic and nonsymbolic numbers in the human brain. *Human Brain Mapping*, 36(2), 475–488. <https://doi.org/10.1002/hbm.22641>
- Lyons, I. M., Ansari, D., & Beilock, S. L. (2015b). Qualitatively different coding of symbolic and nonsymbolic numbers in the human brain. *Human Brain Mapping*, 36(2), 475–488. <https://doi.org/10.1002/hbm.22641>
- Lyons, I. M., & Beilock, S. L. (2018). Characterizing the neural coding of symbolic quantities. *NeuroImage*, 178(May), 503–518. <https://doi.org/10.1016/j.neuroimage.2018.05.062>
- Moyer, R. S., & Landauer, T. K. (1967). Time required for judgment of numerical inequality. *NATURE*, 215, 1519–1520.
- Nieder, A., & Dehaene, S. (2009). Representation of Number in the Brain. *Annual Review of Neuroscience*, 32(1), 185–208. <https://doi.org/10.1146/annurev.neuro.051508.135550>

- Nieder, A., Freedman, D. J., & Miller, E. K. (2002). Representation of the quantity of visual items in the primate prefrontal cortex. *Science*, *297*(5587), 1708–1711.
<https://doi.org/10.1126/science.1072493>
- Nieder, A., & Miller, E. K. (2003). Coding of Cognitive Magnitude: Compressed Scaling of Numerical Information in the Primate Prefrontal Cortex. *Neuron*, *37*(1), 149–157.
[https://doi.org/10.1016/s0896-6273\(02\)01144-3](https://doi.org/10.1016/s0896-6273(02)01144-3)
- Nieder, A., & Miller, E. K. (2004). A parieto-frontal network for visual numerical information in the monkey. *Proceedings of the National Academy of Sciences of the United States of America*, *101*(19), 7457–7462.
<https://doi.org/10.1073/pnas.0402239101>
- Nordt, M., Hoehl, S., & Weigelt, S. (2016). The use of repetition suppression paradigms in developmental cognitive neuroscience. *Cortex*, *80*, 61–75.
<https://doi.org/10.1016/j.cortex.2016.04.002>
- Notebaert, K., Nelis, S., & Reynvoet, B. (2010). The magnitude representation of small and large symbolic numbers in the left and right hemisphere: An event-related fMRI study. *Journal of Cognitive Neuroscience*, *23*(3), 622–630.
<https://doi.org/10.1162/jocn.2010.21445>
- Piazza, M. (2010). Neurocognitive start-up tools for symbolic number representations. *Trends in Cognitive Sciences*, *14*(12), 542–551.
<https://doi.org/10.1016/j.tics.2010.09.008>
- Piazza, M., Izard, V., Pinel, P., Le Bihan, D., & Dehaene, S. (2004). Tuning curves for approximate numerosity in the human intraparietal sulcus. *Neuron*, *44*(3), 547–555.
<https://doi.org/10.1016/j.neuron.2004.10.014>

- Piazza, M., Pinel, P., Le Bihan, D., & Dehaene, S. (2007). A Magnitude Code Common to Numerosities and Number Symbols in Human Intraparietal Cortex. *Neuron*, 53(2), 293–305. <https://doi.org/10.1016/j.neuron.2006.11.022>
- Poldrack, R. A. (2000). Imaging brain plasticity: Conceptual and methodological issues - A theoretical review. *NeuroImage*, 12(1), 1–13. <https://doi.org/10.1006/nimg.2000.0596>
- Reynvoet, B., & Sasanguie, D. (2016). The symbol grounding problem revisited: A thorough evaluation of the ans mapping account and the proposal of an alternative account based on symbol-symbol associations. *Frontiers in Psychology*, 7(OCT), 1–11. <https://doi.org/10.3389/fpsyg.2016.01581>
- Sapountzis, P., Schluppeck, D., Bowtell, R., & Peirce, J. W. (2010). A comparison of fMRI adaptation and multivariate pattern classification analysis in visual cortex. *NeuroImage*, 49(2), 1632–1640. <https://doi.org/10.1016/j.neuroimage.2009.09.066>
- Scheperjans, F., Eickhoff, S. B., Hömke, L., Mohlberg, H., Hermann, K., Amunts, K., & Zilles, K. (2008). Probabilistic maps, morphometry, and variability of cytoarchitectonic areas in the human superior parietal cortex. *Cerebral Cortex*, 18(9), 2141–2157. <https://doi.org/10.1093/cercor/bhm241>
- Scheperjans, F., Hermann, K., Eickhoff, S. B., Amunts, K., Schleicher, A., & Zilles, K. (2008). Observer-independent cytoarchitectonic mapping of the human superior parietal cortex. *Cerebral Cortex*, 18(4), 846–867. <https://doi.org/10.1093/cercor/bhm116>
- Šidák, Z. (1967). Rectangular Confidence Regions for the Means of Multivariate Normal Distributions Author (s): Zbynek Sidak Source : Journal of the American Statistical

- Association , Vol . 62 , No . 318 (Jun ., 1967), pp . Published by : Taylor & Francis , Ltd . on be. *Journal of the American Statistical Association*, 62(318), 626–633.
http://www.jstor.org/stable/2283989?seq=1#page_scan_tab_contents
- Van Opstal, F., Gevers, W., De Moor, W., & Verguts, T. (2008). Dissecting the symbolic distance effect: Comparison and priming effects in numerical and nonnumerical orders. *Psychonomic Bulletin and Review*, 15(2), 419–425.
<https://doi.org/10.3758/PBR.15.2.419>
- Vogel, S. E., Goffin, C., & Ansari, D. (2015). Developmental specialization of the left parietal cortex for the semantic representation of Arabic numerals: An fMR-adaptation study. *Developmental Cognitive Neuroscience*, 12(1), 61–73.
<https://doi.org/10.1016/j.dcn.2014.12.001>
- Vogel, S. E., Goffin, C., Bohnenberger, J., Koschutnig, K., Reishofer, G., Grabner, R. H., & Ansari, D. (2017). The left intraparietal sulcus adapts to symbolic number in both the visual and auditory modalities: Evidence from fMRI. *NeuroImage*, 153(November 2016), 16–27. <https://doi.org/10.1016/j.neuroimage.2017.03.048>
- Wilkey, E. D., & Ansari, D. (2020). Challenging the neurobiological link between number sense and symbolic numerical abilities. *Annals of the New York Academy of Sciences*, 1464(1), 76–98. <https://doi.org/10.1111/nyas.14225>
- Wilkey, E. D., Conrad, B. N., & Price, G. R. (2020). Shared numerosity representations across formats and tasks revealed with 7 Tesla fMRI: decoding, generalization, and individual differences in behavior. In *PREPRINT*.
- Xu, F., & Spelke, E. S. (2000). Large number discrimination in 6-month-old infants. *Cognition*, 74(1), 1–11. [https://doi.org/10.1016/S0010-0277\(99\)00066-9](https://doi.org/10.1016/S0010-0277(99)00066-9)

Yeo, D. J., Wilkey, E. D., & Price, G. R. (2017). The search for the number form area: A functional neuroimaging meta-analysis. *Neuroscience and Biobehavioral Reviews*, 78(January), 145–160. <https://doi.org/10.1016/j.neubiorev.2017.04.027>

7. Appendices

Appendix A. Repeated measured ANOVA (6 Deviants). Within-Subjects Effects.

Similarities between the deviants and the Adaptation numerals were estimated using partial correlations (controlling for catch trials)

VOI	Type III Sum of Squares	df	Mean Square	F	Sig.	Partial Eta Squared
IP1L	0.706	5	0.141	0.786	0.561	0.018
IP1R	0.949	5	0.19	1.087	0.368	0.024
IP2L	1.18	5	0.236	1.347	0.245	0.03
IP2R	3.35	5	0.67	2.574	0.028*	0.055
IP3L	1.106	5	0.221	1.477	0.198	0.032
IP3R	0.147	5	0.029	0.203	0.961	0.005
BS	0.234	5	0.047	0.245	0.942	0.006
CC	0.729	5	0.146	1.397	0.227	0.031
LIPS	1.391	5	0.278	2.261	0.049*	0.049
LTFC	1.151	5	0.23	2.22	0.053	0.048
RIPS	1.179	5	0.236	1.847	0.105	0.04
RMFG	0.957	5	0.191	2.069	0.07	0.045
RMTG	1.278	5	0.256	1.079	0.373	0.024
RT	1.822	5	0.364	1.739	0.127	0.038
RTFC	0.661	5	0.132	1.189	0.316	0.026

* Significant at the uncorrected $p < .05$

** Significant Dunn-Sidak correction; this correction was applied separately for each ROI selection method. For ROIs selected from univariate contrast the corrected threshold was $p < .00568$; for the ROIs selected from probabilistic maps the corrected threshold was $p < .00851$

Appendix B. Within-Subjects Polynomial Contrast, after excluding Deviant 12.

Similarities between the deviants and the Adaptation numerals were estimated using partial correlations (controlling for catch trials)

VOI	Contrast	F	Sig.	Partial Eta Squared
IP1L	Linear	2.461	0.124	0.053
	Quadratic	0.004	0.948	0
IP1R	Linear	0.339	0.563	0.008
	Quadratic	1.621	0.21	0.036
IP2L	Linear	3.573	0.065	0.075
	Quadratic	0.128	0.722	0.003
IP2R	Linear	2.901	0.096	0.062
	Quadratic	5*	0.03	0.102
IP3L	Linear	2.707	0.107	0.058
	Quadratic	0.076	0.784	0.002
IP3R	Linear	0.043	0.838	0.001
	Quadratic	0.143	0.707	0.003
BS	Linear	0.759	0.388	0.017
	Quadratic	0.041	0.84	0.001
CC	Linear	2.093	0.155	0.045
	Quadratic	0.421	0.52	0.009
LIPS	Linear	4.936*	0.031	0.101
	Quadratic	4.38	0.044	0.089
LTFC	Linear	5.198*	0.028	0.106
	Quadratic	1.356	0.251	0.03
RIPS	Linear	2.93	0.094	0.062
	Quadratic	1.974	0.167	0.043
RMFG	Linear	0.221	0.64	0.005
	Quadratic	8.995**	0.004	0.17
RMTG	Linear	3.661	0.062	0.077
	Quadratic	0.007	0.935	0
RT	Linear	2.055	0.159	0.045
	Quadratic	0.335	0.566	0.008
RTFC	Linear	0.14	0.71	0.003
	Quadratic	2.771	0.103	0.059

* Significant at the uncorrected $p < .05$

** Significant Dunn-Sidak correction; this correction was applied separately for each ROI selection method. For ROIs selected from univariate contrast the corrected threshold was $p < .00568$; for the ROIs selected from probabilistic maps the corrected threshold was $p < .00851$

Appendix C. Within-Subjects Polynomial Contrast using zero-order correlations to estimate similarities

VOI	Contrast	F	Sig.	Partial Eta Squared
IP1L	Linear	4.157*	0.047	0.086
	Quadratic	0	0.984	0
IP1R	Linear	0.253	0.617	0.006
	Quadratic	3.228	0.079	0.068
IP2L	Linear	2.511	0.12	0.054
	Quadratic	0.073	0.788	0.002
IP2R	Linear	3.567	0.066	0.075
	Quadratic	5.792*	0.02	0.116
IP3L	Linear	1.57	0.217	0.034
	Quadratic	0.007	0.932	0
IP3R	Linear	0.041	0.841	0.001
	Quadratic	0.135	0.715	0.003
BS	Linear	0.843	0.364	0.019
	Quadratic	0.001	0.979	0
CC	Linear	0.642	0.427	0.014
	Quadratic	0.337	0.564	0.008
LIPS	Linear	4.281*	0.044	0.089
	Quadratic	4.654*	0.036	0.096
LTFC	Linear	3.53	0.067	0.074
	Quadratic	0.312	0.579	0.007
RIPS	Linear	4.697*	0.036	0.096
	Quadratic	1.604	0.212	0.035
RMFG	Linear	1.168	0.286	0.026
	Quadratic	8.65**	0.005	0.164
RMTG	Linear	2.271	0.139	0.049
	Quadratic	0.069	0.794	0.002
RT	Linear	0.652	0.424	0.015
	Quadratic	0.009	0.925	0
RTFC	Linear	0.061	0.806	0.001
	Quadratic	2.304	0.136	0.05

* Significant at the uncorrected $p < .05$

** Significant Dunn-Sidak correction; this correction was applied separately for each ROI selection method. For ROIs selected from univariate contrast the corrected threshold was $p < .00568$; for the ROIs selected from probabilistic maps the corrected threshold was $p < .00851$

Appendix D. Within-Subjects Polynomial Contrast interaction with Age, after excluding Deviant 12.

Similarities between the deviants and the Adaptation numerals were estimated using partial correlations (controlling for catch trials)

VOI	Source	Contrast	F	Sig.	Partial Eta Squared
IP1L	Deviants * Age_Years	Linear	1.137	0.363	0.202
		Quadratic	0.525	0.83	0.104
IP1R	Deviants * Age_Years	Linear	0.955	0.486	0.175
		Quadratic	0.42	0.901	0.085
IP2L	Deviants * Age_Years	Linear	1.028	0.434	0.186
		Quadratic	0.508	0.842	0.101
IP2R	Deviants * Age_Years	Linear	0.861	0.557	0.161
		Quadratic	2.07	0.065	0.315
IP3L	Deviants * Age_Years	Linear	0.422	0.9	0.086
		Quadratic	0.973	0.472	0.178
IP3R	Deviants * Age_Years	Linear	0.54	0.818	0.107
		Quadratic	0.816	0.593	0.154
BS	Deviants * Age_Years	Linear	2.115	0.06	0.32
		Quadratic	0.97	0.474	0.177
CC	Deviants * Age_Years	Linear	0.819	0.591	0.154
		Quadratic	2.089	0.063	0.317
LIPS	Deviants * Age_Years	Linear	0.483	0.86	0.097
		Quadratic	0.623	0.753	0.122
LTFC	Deviants * Age_Years	Linear	1.267	0.291	0.22
		Quadratic	0.908	0.521	0.168
RIPS	Deviants * Age_Years	Linear	1.046	0.422	0.189
		Quadratic	0.837	0.577	0.157
RMFG	Deviants * Age_Years	Linear	2.452*	0.031	0.353
		Quadratic	0.506	0.843	0.101
RMTG	Deviants * Age_Years	Linear	0.441	0.888	0.089
		Quadratic	1.184	0.336	0.208
RT	Deviants * Age_Years	Linear	0.891	0.534	0.165
		Quadratic	0.782	0.621	0.148
RTFC	Deviants * Age_Years	Linear	0.494	0.853	0.099
		Quadratic	0.776	0.626	0.147

* Significant at the uncorrected $p < .05$

** Significant Dunn-Sidak correction; this correction was applied separately for each ROI selection method. For ROIs selected from univariate contrast the corrected threshold was $p < .00568$; for the ROIs selected from probabilistic maps the corrected threshold was $p < .00851$

Appendix E. Within-Subjects Polynomial Contrast interaction with Age, using zero-order correlations to estimate similarities.

VOI	Source	Deviants	F	Sig.	Partial Eta Squared
IP1L	Deviants * Age_Years	Linear	0.625	0.751	0.122
		Quadratic	0.418	0.903	0.085
IP1R	Deviants * Age_Years	Linear	1.182	0.337	0.208
		Quadratic	0.371	0.929	0.076
IP2L	Deviants * Age_Years	Linear	0.776	0.626	0.147
		Quadratic	0.33	0.949	0.068
IP2R	Deviants * Age_Years	Linear	0.724	0.669	0.139
		Quadratic	1.595	0.161	0.262
IP3L	Deviants * Age_Years	Linear	0.228	0.983	0.048
		Quadratic	0.747	0.65	0.142
IP3R	Deviants * Age_Years	Linear	0.62	0.755	0.121
		Quadratic	1.037	0.427	0.187
BS	Deviants * Age_Years	Linear	1.545	0.176	0.256
		Quadratic	0.595	0.776	0.117
CC	Deviants * Age_Years	Linear	1.265	0.292	0.219
		Quadratic	1.684	0.136	0.272
LIPS	Deviants * Age_Years	Linear	0.555	0.807	0.11
		Quadratic	0.852	0.565	0.159
LTFC	Deviants * Age_Years	Linear	2.052	0.068	0.313
		Quadratic	0.546	0.814	0.108
RIPS	Deviants * Age_Years	Linear	1.512	0.187	0.252
		Quadratic	0.641	0.738	0.125
RMFG	Deviants * Age_Years	Linear	1.178	0.339	0.207
		Quadratic	1.168	0.344	0.206
RMTG	Deviants * Age_Years	Linear	0.977	0.469	0.178
		Quadratic	0.909	0.52	0.168
RT	Deviants * Age_Years	Linear	0.987	0.462	0.18
		Quadratic	0.409	0.908	0.083
RTFC	Deviants * Age_Years	Linear	0.518	0.835	0.103
		Quadratic	1.009	0.447	0.183

Appendix F. Ratio and Frequency Model fit, after excluding Deviant 12.

Similarities between the deviants and the Adaptation numerals were estimated using partial correlations (controlling for catch trials)

ROI	Ratio Model Fit				Frequency Model Fit			
	t	p	d	BF ₀₁	t	p	d	BF ₀₁
IP1L	1.353	0.183	0.202	2.644	0.702	0.487	0.105	4.908 [†]
IP1R	-0.458	0.649	-0.068	5.604 [†]	0.112	0.911	0.017	6.152 [†]
IP2L	0.886	0.380	0.132	4.279 [†]	1.068	0.291	0.159	3.630 [†]
IP2R	-0.381	0.705	-0.057	5.778 [†]	0.703	0.486	0.105	4.903 [†]
IP3L	0.257	0.798	0.038	5.999 [†]	0.398	0.692	0.059	5.741 [†]
IP3R	0.106	0.916	0.016	6.156 [†]	-0.162	0.872	-0.024	6.112 [†]
BS	0.566	0.574	0.084	5.319 [†]	1.546	0.129	0.230	2.053
CC	0.271	0.787	0.040	5.977 [†]	-0.015	0.988	-0.002	6.188 [†]
LIPS	0.461	0.647	0.069	5.597 [†]	0.531	0.598	0.079	5.416 [†]
LTFC	0.311	0.757	0.046	5.912 [†]	1.880	0.067	0.280	1.235
RIPS	1.077	0.287	0.161	3.599 [†]	0.108	0.915	0.016	6.155 [†]
RMFG	0.279	0.781	0.042	5.964 [†]	0.262	0.794	0.039	5.990 [†]
RMTG	1.731	0.090	0.258	1.565	0.668	0.508	0.100	5.015 [†]
RT	1.186	0.242	0.177	3.210 [†]	0.686	0.496	0.102	4.957 [†]
RTFC	0.940	0.352	0.140	4.089 [†]	0.208	0.836	0.031	6.063 [†]

[†] Bayes Factor indicating substantial support for the null

Appendix G. Ratio and Frequency Model fit, using zero-order correlations to estimate similarity

ROI	Ratio Model Fit				Frequency Model Fit			
	t	p	d	BF ₀₁	t	p	d	BF ₀₁
IP1L	1.207	0.234	0.180	3.139 [†]	0.622	0.537	0.093	5.156 [†]
IP1R	-1.883	0.066	-0.281	1.228	-1.180	0.244	-0.176	3.231 [†]
IP2L	-0.609	0.546	-0.091	5.195 [†]	2.278*	0.028	0.340	0.603
IP2R	-1.328	0.191	-0.198	2.727	0.369	0.714	0.055	5.803 [†]
IP3L	-0.983	0.331	-0.146	3.936 [†]	-0.496	0.622	-0.074	5.509 [†]
IP3R	-2.301*	0.026	-0.343	0.578	-1.190	0.240	-0.177	3.197 [†]
BS	0.306	0.761	0.046	5.921 [†]	1.717	0.093	0.256	1.599
CC	-0.630	0.532	-0.094	5.132 [†]	-1.380	0.175	-0.206	2.558
LIPS	-0.090	0.929	-0.013	6.165 [†]	-0.466	0.643	-0.070	5.584 [†]
LTFC	-0.345	0.732	-0.051	5.850 [†]	1.074	0.289	0.160	3.608 [†]
RIPS	-0.202	0.841	-0.030	6.070 [†]	-0.959	0.343	-0.143	4.021 [†]
RMFG	-0.430	0.670	-0.064	5.672 [†]	-0.684	0.497	-0.102	4.963 [†]
RMTG	-0.374	0.710	-0.056	5.792 [†]	-0.907	0.369	-0.135	4.205 [†]
RT	-1.526	0.134	-0.228	2.109	1.029	0.309	0.153	3.771 [†]
RTFC	0.265	0.792	0.040	5.987 [†]	-0.722	0.474	-0.108	4.843 [†]

[†] Bayes Factor indicating substantial support for the null

* Significant at the uncorrected $p < .05$

** Significant Dunn-Sidak correction; this correction was applied separately for each ROI selection method. For ROIs selected from univariate contrast the corrected threshold was $p < .00568$; for the ROIs selected from probabilistic maps the corrected threshold was $p < .00851$

Appendix H. Ratio and Frequency Model fit interaction with Age, after excluding Deviant 12.

Similarities between the deviants and the Adaptation numerals were estimated using partial correlations (controlling for catch trials)

ROI	Ratio Model Fit ~ Age			Frequency Model Fit ~ Age		
	r	p	BF	r	p	BF
IP1L	0.375	0.011	0.237	-0.121	0.427	3.966 [†]
IP1R	0.154	0.312	3.277	0.116	0.449	4.076 [†]
IP2L	-0.064	0.678	4.951	0.153	0.316	3.306 [†]
IP2R	0.008	0.960	5.376	-0.012	0.939	5.367 [†]
IP3L	0.161	0.290	3.129	0.196	0.198	2.410
IP3R	0.404**	0.006	0.138	0.038	0.806	5.277 [†]
BS	0.060	0.695	4.996	-0.096	0.531	4.448 [†]
CC	0.068	0.658	4.895	0.035	0.820	5.249 [†]
LIPS	0.019	0.904	5.344	0.131	0.393	3.777 [†]
LTFC	0.327*	0.028	0.525	-0.052	0.734	5.090 [†]
RIPS	0.064	0.675	4.941	-0.022	0.884	5.327 [†]
RMFG	0.121	0.427	3.966	0.311*	0.038	0.662
RMTG	0.376*	0.011	0.233	-0.049	0.751	5.126 [†]
RT	0.203	0.180	2.253	-0.128	0.400	3.821 [†]
RTFC	0.022	0.886	5.329	-0.216	0.155	2.019

[†] Bayes Factor indicating substantial support for the null

* Significant at the uncorrected $p < .05$

** Significant Dunn-Sidak correction; this correction was applied separately for each ROI selection method. For ROIs selected from univariate contrast the corrected threshold was $p < .00568$; for the ROIs selected from probabilistic maps the corrected threshold was $p < .00851$

Appendix I. Ratio and Frequency Model fit interaction with Age, using zero-order correlations to estimate similarity.

ROI	Ratio Model Fit ~ Age			Frequency Model Fit ~ Age		
	r	p	BF	r	p	BF
IP1L	0.200	0.187	2.314	-0.217	0.153	1.996
IP1R	0.164	0.281	3.067	0.074	0.629	4.808 [†]
IP2L	0.214	0.158	2.050	0.101	0.510	4.363 [†]
IP2R	0.169	0.266	2.959	-0.043	0.779	5.180 [†]
IP3L	0.129	0.399	3.814	0.164	0.282	3.069 [†]
IP3R	0.427**	0.003	0.086	0.066	0.668	4.923 [†]
BS	0.088	0.567	4.593	0.133	0.385	3.735 [†]
CC	0.156	0.306	3.238	-0.115	0.451	4.089 [†]
LIPS	0.084	0.584	4.653	0.145	0.343	3.479 [†]
LTFC	0.398*	0.007	0.154	-0.011	0.943	5.369 [†]
RIPS	0.141	0.354	3.551	-0.063	0.683	4.964 [†]
RMFG	0.066	0.668	4.923	0.126	0.411	3.879 [†]
RMTG	0.320*	0.032	0.586	0.048	0.753	5.129 [†]
RT	0.486**	0.001	0.021	0.004	0.979	5.380 [†]
RTFC	0.095	0.534	4.463	-0.213	0.161	2.076

[†] Bayes Factor indicating substantial support for the null

* Significant at the uncorrected $p < .05$

** Significant Dunn-Sidak correction; this correction was applied separately for each ROI selection method. For ROIs selected from univariate contrast the corrected threshold was $p < .00568$; for the ROIs selected from probabilistic maps the corrected threshold was $p < .00851$

8. Curriculum Vitae

Name:	Aymee Alvarez Rivero
Post-Secondary Education and Degrees	<p>2008-present MSc. Psychology University of Western Ontario Havana, Cuba.</p> <p>2008-2013 B.Sc. Psychology University of Havana. Havana, Cuba.</p>
Honours and Awards:	Western International Graduate Student Award Sept 2018 to August 2020
Related Work Experience	<p>Teaching Assistant University of Western Ontario 2018 - 2020</p> <p>Junior Research Assistant Cuban Neurosciences Center 2013 - 2018</p>
Publications	<p>Reigosa-Crespo, V., Castro-Cañizares, D., Estevez-Perez, N., Santos, E., Torres Díaz, R., Mosquera, R., Alvarez, A., Recio, B., Gonzalez, E., Amor, V., Ontivero, M., Valdés-Sosa, M. (2020) Numerical skills and dyscalculia. From basic research to practice in Cuba. <i>Studies in Psychology</i>, 41(2). 373-403. https://doi.org/10.1080/02109395.2020.1749502</p> <p>Torres Díaz, R., Mosquera, R., Ontivero, M., Romero, Y, Alvarez, A., González-Alemañy, E., Ojeda, J.A., Peón, B., Recio, B., Valdés-Sosa, M. (2020). Text segmentation ability predicts future reading efficiency in Spanish-speaking children. <i>Acta Psychologica</i>, 204. 103015. https://doi.org/10.1016/j.actpsy.2020.103015</p> <p>Santos-Febles, E., Reigosa-Crespo, V., García-Liashenko, K., Echemendía, A., Plasencia, E., Pujols, G., Alvarez, A., Eimil, E. (2015). A System to Support Regional Screening Programs to Identify School-age Children at Risk of Neurodevelopmental Disorders. <i>World Congress on Medical Physics and Biomedical Engineering, June 7-12, 2015, Toronto, Canada</i>. 1469-1473. https://doi.org/10.1007/978-3-319-19387-8_358</p>